



This is a repository copy of *Search for quantum black hole production in lepton + jet final states using proton-proton collisions at $\sqrt{s}=13$ TeV with the ATLAS detector.*

White Rose Research Online URL for this paper:

<https://eprints.whiterose.ac.uk/210749/>

Version: Published Version

Article:

Aad, G. orcid.org/0000-0002-6665-4934, Abbott, B. orcid.org/0000-0002-5888-2734, Abbott, D.C. orcid.org/0000-0002-7248-3203 et al. (2920 more authors) (2024) Search for quantum black hole production in lepton + jet final states using proton-proton collisions at $\sqrt{s}=13$ TeV with the ATLAS detector. *Physical Review D*, 109. 032010. ISSN 2470-0010

<https://doi.org/10.1103/physrevd.109.032010>

Reuse

This article is distributed under the terms of the Creative Commons Attribution (CC BY) licence. This licence allows you to distribute, remix, tweak, and build upon the work, even commercially, as long as you credit the authors for the original work. More information and the full terms of the licence here:

<https://creativecommons.org/licenses/>

Takedown

If you consider content in White Rose Research Online to be in breach of UK law, please notify us by emailing eprints@whiterose.ac.uk including the URL of the record and the reason for the withdrawal request.



eprints@whiterose.ac.uk
<https://eprints.whiterose.ac.uk/>

Search for quantum black hole production in lepton + jet final states using proton-proton collisions at $\sqrt{s} = 13$ TeV with the ATLAS detector

G. Aad *et al.**
(ATLAS Collaboration)

 (Received 28 July 2023; accepted 1 December 2023; published 27 February 2024)

A search for quantum black holes in electron + jet and muon + jet invariant mass spectra is performed with 140 fb^{-1} of data collected by the ATLAS detector in proton-proton collisions at $\sqrt{s} = 13$ TeV at the Large Hadron Collider. The observed invariant mass spectrum of lepton + jet pairs is consistent with Standard Model expectations. Upper limits are set at 95% confidence level on the production cross section times branching fractions for quantum black holes decaying into a lepton and a quark in a search region with invariant mass above 2.0 TeV. The resulting quantum black hole lower mass threshold limit is 9.2 TeV in the Arkani-Hamed-Dimopoulos-Dvali model, and 6.8 TeV in the Randall-Sundrum model.

DOI: [10.1103/PhysRevD.109.032010](https://doi.org/10.1103/PhysRevD.109.032010)

I. INTRODUCTION

Quantum black holes (QBHs) are predicted in low-scale quantum gravity models [1–3] that offer solutions to the mass hierarchy problem of the Standard Model (SM) by lowering the scale of quantum gravity (M_D) from the high Planck scale ($\sim 10^{16}$ TeV) to the TeV region (1–10 TeV). In these new physics scenarios, gravity becomes strong, and quantum effects are relevant. In models with large extra dimensions such as the Arkani-Hamed-Dimopoulos-Dvali (ADD) model [1,2], the gravitational field is allowed to propagate in n extra dimensions ($n = 6$ in our analysis), while all SM fields are localized in the usual four-dimensional space-time. There are also warped scenarios, such as the Randall-Sundrum model (RS1) [3], in which a single warped extra dimension ($n = 1$) separates two three-dimensional branes by some distance. Gravitons can propagate in this warped dimension, and the effective Planck scale on the three-dimensional brane is determined by the curvature of the extra dimension, also referred to as the warp factor. These models postulate conservation of total angular momentum, color, and electric charge in the production and in the decay of QBHs [4–6]. The behavior of QBHs with masses near M_D decaying into two-particle final state is distinct from that of the semiclassical black holes [7] that decay into a multiparticle final state via Hawking radiation [8–11] (thermal decay). Two-particle

final states make up 51% (74%) of all possible QBH decays in the ADD (RS1) model [6].

The QBH models can be tested at the Large Hadron Collider (LHC) up to 13 TeV. In this paper, a search for QBHs decaying into a single electron (e) or a single muon (μ), and a quark producing a jet is undertaken. The QBHs are postulated to be produced near the low-scale M_D . One expects in strong-gravity interactions that angular momentum, electric charge, and color are conserved. It is less clear that global symmetries such as baryon or lepton number of the SM need to be conserved in strong-gravity interactions. While in high Planck-scale gravity in four dimensions the baryon number violation is bound to be very small [6], the baryon number violation in low-scale gravity in higher dimensions is less constrained and could cause a sizeable impact on observables. Therefore, a search for QBH production that violates SM global symmetries provides a possible way to examine low-scale gravity phenomena. In the absence of a coherent and reliable Feynman diagram technique for the quantum black hole description, the easiest and most accurate way to visualize the QBH production mechanism would be a set of partonic 2-to-2 scattering processes,

$$uu \rightarrow \bar{d}\ell^+, \quad ud \rightarrow \bar{u}\ell^+, \quad \bar{d}\bar{d} \rightarrow d\ell^+, \quad (1)$$

and the respective charge conjugates. Only these six electric charge initial states ($\pm 4/3, \pm 2/3, \pm 1/3$) can result in a lepton-quark or lepton-antiquark pair in the final state. Here, the u and d symbols denote all up and down quark flavors and ℓ —all charged leptons excluding τ -lepton, which is not considered in the analysis. In this way, all quark flavors are possible in both the initial and the final state in Eq. (1). The angular momentum of the QBH is entirely due to the spin states of the incoming partons.

*Full author list given at the end of the article.

Published by the American Physical Society under the terms of the [Creative Commons Attribution 4.0 International license](https://creativecommons.org/licenses/by/4.0/). Further distribution of this work must maintain attribution to the author(s) and the published article's title, journal citation, and DOI. Funded by SCOAP³.

The initial orbital angular momentum is assumed to be negligible because of the small impact parameter in the parton-parton collision. The model/generator makes no attempt to convert a classical impact parameter to quantized orbital angular momentum. Final states with lepton plus quark (antiquark) can only have either the spin 0 or the spin 1. Thus, only QBHs with these spin states can contribute to the cross section of the considered process. Color is conserved in the interaction, but QBH has color, and thus the final state has color, so the beam remnant has the corresponding anticolor.

A previous search for QBHs in the lepton + jet channel was performed in proton-proton (p - p) collisions at a center-of-mass energy of $\sqrt{s} = 8$ TeV by ATLAS [12]. The combined 95% confidence level upper limit on the QBH production cross section with threshold mass above 3.5 TeV was found to be 0.18 fb. This limit constrains the threshold mass of QBH, which was found to be above 5.3 TeV in the ADD model. QBHs have also been sought in the dijet, dilepton, and photon + jet channels by both ATLAS and CMS at center-of-mass energies of 7 TeV [13–15], 8 TeV [16–20], and 13 TeV [21–27]. These LHC results with different final states use the same QBH model/generator, so results can be compared. In general, the QBH searches in the lepton + jet final-state are less sensitive than in the dijet searches (at the same QBH threshold mass). On the other hand, the limits obtained in the lepton + jet events are stronger than those with photon + jet and dilepton final states. Different final states supplement each other because they search for QBHs with different quantum numbers. In addition, the lepton + jet model-independent limits can constrain some other models violating the baryon-lepton global symmetry.

II. ATLAS DETECTOR

The ATLAS experiment [28] at the LHC is a multipurpose particle detector with a forward-backward symmetric cylindrical geometry and a nearly 4π coverage in solid angle.¹ It consists of an inner tracking detector surrounded by a thin superconducting solenoid providing a 2 T axial magnetic field, electromagnetic and hadron calorimeters, and a muon spectrometer. The inner tracking detector covers the pseudorapidity range $|\eta| < 2.5$. It consists of silicon pixel [29], silicon microstrip, and transition radiation tracking detectors. Lead/liquid-argon (LAr) sampling calorimeters provide electromagnetic (EM) energy

¹ATLAS uses a right-handed coordinate system with its origin at the nominal interaction point (IP) in the center of the detector and the z -axis along the beam pipe. The x -axis points from the IP to the center of the LHC ring, and the y -axis points upward. Cylindrical coordinates (r, ϕ) are used in the transverse plane, ϕ being the azimuthal angle around the z -axis. The pseudorapidity is defined in terms of the polar angle θ as $\eta = -\ln \tan(\theta/2)$. Angular distance is measured in units of $\Delta R \equiv \sqrt{(\Delta\eta)^2 + (\Delta\phi)^2}$.

measurements with high granularity. A steel/scintillator-tile hadron calorimeter covers the central pseudorapidity range ($|\eta| < 1.7$). The end cap and forward regions are instrumented with LAr calorimeters for both the EM and hadronic energy measurements up to $|\eta| = 4.9$. The muon spectrometer surrounds the calorimeters and is based on three large superconducting air-core toroidal magnets with eight coils each. The field integral of the toroids ranges between 2.0 and 6.0 Tm across most of the detector. The muon spectrometer includes a system of precision tracking chambers and fast detectors for triggering. A two-level trigger system [30] is used to select events. The first-level trigger is implemented in hardware and uses a subset of the detector information to accept events at a rate below 100 kHz. This is followed by a software-based trigger that reduces the accepted event rate to 1 kHz on average depending on the data-taking conditions. An extensive software suite [31] is used in data simulation, in the reconstruction and analysis of real and simulated data, in detector operations, and in the trigger and data acquisition systems of the experiment.

III. DATASETS AND SIMULATED EVENT SAMPLES

The results described in this paper use p - p collision data collected by ATLAS at $\sqrt{s} = 13$ TeV during 2015–2018 in stable beam conditions and with all detector systems operating normally [32]. The event quality is checked to remove events with noise bursts or coherent noise in the calorimeters. Events in the electron channel are required to pass at least one of two single-electron triggers [33]: the first requires a transverse momentum (p_T) threshold of 60 GeV, and the second has looser identification criteria and a p_T threshold of 120 or 140 GeV, depending on the data-taking period. Events in the muon channel are recorded using a single-muon trigger [34] with a transverse momentum (p_T) requirement of at least 50 GeV. The integrated luminosity of the dataset is determined to be $140.1 \pm 1.2 \text{ fb}^{-1}$ [35], obtained using the LUCID-2 detector [36] for the primary luminosity measurements.

Background events with a high- p_T lepton and one or more jets arise from electroweak processes including vector boson production with additional jets ($W/Z + \text{jets}$), dibosons (WW , WZ and ZZ), top-quark pair ($t\bar{t}$) and single-top-quark production, and multijet processes including nonprompt leptons from leptonic hadron decays and jets misidentified as leptons.

Monte Carlo (MC) simulation is used to model the expected contributions of various SM processes as well as possible QBH signals. A full description of the MC simulated event samples used is given below and summarized in Table I. The expected contributions of the SM backgrounds reported in Table I are taken from MC simulation, either directly or adjusted by the fit to data in dedicated control regions. The multijet background is

TABLE I. The event generators used for simulation of the signal and background processes. The acronyms ME and PS stand for matrix element and parton shower. The top-quark mass is set to 172.5 GeV.

Process	ME generator and ME PDFs	PS, PDFs, nonperturbative effect
$W/Z + \text{jets}$	Sherpa 2.2.1, NNPDF3 . 0NLO	Sherpa 2.2.1, NNPDF3 . 0NLO
$t\bar{t}$	POWHEG BOX, NNPDF3 . 0NLO	PYTHIA 8.230, NNPDF2 . 3LO, EvtGen 1.6.0
Single-top s -channel, tW	POWHEG BOX, NNPDF3 . 0NLO	PYTHIA 8.230, NNPDF2 . 3LO, EvtGen 1.6.0
Single-top t -channel	POWHEG BOX, NNPDF3 . 04fNLO, MadSpin	PYTHIA 8.230, NNPDF2 . 3LO, EvtGen 1.6.0
Diboson, semileptonic decay	Sherpa 2.2.1, NNPDF3 . 0NLO	Sherpa 2.2.1, NNPDF3 . 0NLO
Diboson, fully leptonic decay	Sherpa 2.2.2, NNPDF3 . 0NLO	Sherpa 2.2.2, NNPDF3 . 0NLO
QBH signal, ADD, RS1	QBH 3.0, CTEQ6L1	PYTHIA 8.205, CTEQ6L1, EvtGen 1.2.0

measured directly in data. In this case the events collected by a set of unrescaled single-lepton triggers with different p_T -thresholds are used.

$W/Z + \text{jets}$ and diboson samples [37,38] are simulated with the Sherpa generator [39]. The $W/Z + \text{jets}$, and semi-leptonically decaying diboson samples, are simulated with Sherpa 2.2.1, while the fully leptonic diboson processes are simulated with Sherpa 2.2.2. In the Sherpa samples the additional hard parton emissions [40] are matched to parton showers based on Catani–Seymour dipole factorization [41]. The NNPDF3 . 0NLO [42] set of parton distribution functions (PDFs) and a dedicated set of tuned parameters developed by the Sherpa authors are used [39]. The matching of the matrix element to the parton shower [43–46] is employed for the various jet multiplicities, which are then merged into an inclusive sample using an improved CKKW (Catani–Krauss–Kuhn–Webber) procedure [45] that is extended to next-to-leading-order (NLO) accuracy using the MEPS@NLO prescription [44]. The virtual QCD correction for matrix elements at NLO accuracy is provided by the OpenLoops library [47,48]. The $W/Z + \text{jets}$ (diboson) simulations are calculated for up to two (one) additional partons at NLO and up to four (three) additional partons at Leading Order (LO). The $W/Z + \text{jets}$ processes are normalized to a next-to-next-to-leading-order (NNLO) cross section prediction [49]. The diboson processes are normalized to the NNLO cross section prediction [50] as well.

The production of $t\bar{t}$ [51] and single-top tW [52] and s -channel [53] events is modeled using the POWHEG BOX [54–56] v2 generator at NLO with the NNPDF3 . 0NLO PDF set. The single-top t -channel [57] is modeled with POWHEG BOX in the four-flavor scheme with the NNPDF3 . 04fNLO PDF set. The events are interfaced with PYTHIA 8.230 [58] using the A14 tune [59] and the NNPDF2 . 3LO PDF set [60]. The h_{damp} parameter² is set to 1.5 times the top-quark mass [61]. The $t\bar{t}$ inclusive production cross section is corrected to the theory prediction at NNLO in QCD, including the resummation of

²The h_{damp} parameter controls the p_T of the first additional emission beyond the leading-order Feynman diagram in the parton shower and therefore regulates the high- p_T emission against which the $t\bar{t}$ system recoils.

next-to-next-to-leading logarithmic (NNLL) soft-gluon terms calculated using Top++2.0 [62]. The tW inclusive cross section is corrected to the theory prediction calculated at NLO in QCD with NNLL soft-gluon corrections [63,64]. The MadSpin [65] generator is used to preserve top-quark spin correlations in the t channel of the single-top background. The EvtGen 1.6.0 [66] package is applied for the modeling of c - and b -hadron decays.

The simulated QBH signal event samples are obtained from the QBH 3.0 generator [67], which uses the CTEQ6L1 leading-order PDF set [59,68]. The parton showering and hadronization are performed in PYTHIA 8.205, using the CTEQ6L1 PDF set and the A14 tune. The QCD factorization scale for the PDFs is set to the inverse gravitational radius [67]. The QBH simulation assumes massless parton interaction and conserves total angular momentum. The threshold mass, M_{th} , is set equal to M_{D} . For the ADD QBH signal, the number of extra dimensions is $n = 6$ (total number of dimensions $D = 10$). For the RS1 QBH signal, a single extra dimension is assumed leading to a total of five dimensions. The ADD (RS1) samples for both leptonic channels are generated with M_{th} from 2 TeV to 9.5 (7.5) TeV with steps of 0.5 TeV (the same as in Ref. [12]). A quantum black hole is not a particle, so it does not have a single mass or width. The generator produces a distribution of QBH masses (with no additional mass smearing). The QBH mass is required to be in range of 1–3 M_{D} to ensure that the QBHs are produced in the region in which expected quantum effects are important, and that a region of possible thermal decay is excluded. The decay products have exactly the energy and momentum of the produced black hole. Unlike particles produced in quantum field theory, the black hole is produced in a nonperturbative gravity model. The cross sections predicted by the QBH 3.0 event generator [67] are used in the determination of the model-dependent limits for the signal processes. Processes with a quark pair in the initial state have at least 2 orders of magnitude higher cross sections than those with antiquark pairs in the initial state.

All simulated event samples include the effect of multiple p - p interactions in the same or neighboring bunch crossings. These effects are collectively referred to as pileup. The simulation of pile-up collisions is performed

with PYTHIA 8.186 using the ATLAS A3 set of tuned parameters [69] and the NNPDF2.3LO PDF set and weighted to reproduce the average number of pile-up interactions per bunch crossing observed in data. The generated background events are passed through a full detector simulation [70] based on GEANT4 [71]. Simulated QBH event samples are produced with a fast parametrization of the calorimeter response [72], while GEANT4 is used for the other detector systems.

IV. EVENT RECONSTRUCTION AND OBJECT IDENTIFICATION

For an event to be considered, at least one p - p interaction vertex with at least two tracks must be reconstructed. The primary vertex is chosen to be the vertex with the highest summed p_T^2 of tracks with transverse momentum $p_T > 0.4$ GeV that are associated with the vertex [73].

Two identification levels are defined for leptons and jets, referred to as “Baseline” and “Signal,” with Signal objects being a subset of Baseline. The Baseline requirement provides a higher selection efficiency for leptons and jets when calculating missing transverse momentum and resolving ambiguities between overlapping physics objects (see below in this section). The leading lepton passing the Signal selection is matched to the lepton that triggered the event.

Electron candidates are reconstructed using energy clusters in the EM calorimeter which are matched to a track of Inner Detector (ID) track, and they are calibrated as described in Ref. [74]. Baseline electron candidates are required to have $|\eta| < 2.47$ in order to pass through the fine-granularity region of the EM calorimeter and be outside the range $1.37 < |\eta| < 1.52$ corresponding to the transition region between the barrel and end cap EM calorimeters. They should also satisfy Loose identification criteria and have $p_T > 10$ GeV. The trajectory of Baseline electrons must be consistent with the primary vertex to suppress electrons originating from pileup. Therefore, the tracks associated with Baseline electrons must have a longitudinal impact parameter relative to the primary vertex (z_0) such that $|z_0 \cdot \sin\theta| < 0.5$ mm. Signal electrons are defined as Baseline candidates that have $p_T > 30$ GeV and satisfy the Tight identification and HighPtCaloOnly isolation requirements [74]. The track associated with each Signal electron must have a transverse impact parameter significance $|d_0/\sigma(d_0)| \leq 5$.

Baseline muon candidates are reconstructed in the region $|\eta| < 2.5$ by matching ID tracks to tracks reconstructed in the Muon Spectrometer, and they are calibrated *in situ* using $Z \rightarrow \mu\mu$ decays [75]. Baseline muon candidates are required to have $p_T > 10$ GeV. They have to satisfy a set of requirements on the quality of the tracks defined as Medium [75] and to pass a requirement on the longitudinal impact parameter $|z_0 \cdot \sin\theta| < 0.5$ mm. Signal muons are defined as Baseline candidates that

have $p_T > 30$ GeV, pass a requirement on the significance of transverse impact parameter $|d_0/\sigma(d_0)| \leq 3$, and satisfy HighPt muon identification requirements [75] and a track-based isolation criterion. For the isolation requirement, the summed p_T of tracks (with $p_T > 0.4$ GeV) originating from the primary vertex within a cone of radius $\Delta R = 0.2$ around the muon, but excluding the muon candidate track itself, has to be less than 1.25 GeV. A bad-muon veto for the HighPt muons is applied. An event is rejected when Signal muon has a large relative error of charge over momentum (q/p) associated with the track. The veto requirement is changing from 2.5σ to 2.0σ depending on the muon η for the muon $p_T \leq 1$ TeV, and is linearly tightened to 1σ for muons with $p_T \geq 5$ TeV. The σ is the average expected error on the (q/p) as a function of the muon p_T and η .

The anti- k_t algorithm [76] with distance parameter $R = 0.4$ implemented in the FastJet library [77] is used to reconstruct jets up to $|\eta| = 4.9$ from massless clusters of energy depositions in the calorimeter [78] (EMTopo jets). Jets are then calibrated as described in Refs. [79,80]. Baseline jets are required to have $p_T > 20$ GeV and $|\eta| < 2.8$. Events are vetoed if they contain jets induced by calorimeter noise or noncollision background, according to criteria described in Ref. [81]. Additional jets that arise from pile-up interactions are rejected by applying a dedicated track-based selection (Jet Vertex Tagger [82]), based on classifying the tracks associated with the jet as pointing or not pointing to the primary vertex. The jet candidates passing all the above requirements are called Baseline jets. Signal jets are defined as Baseline candidates that have $p_T > 30$ GeV.

Jets containing b -flavored hadrons, used only for the estimation of some backgrounds, are identified in the region $|\eta| < 2.5$ by the MV2c10 algorithm [83], which makes use of the impact parameters of tracks associated with the candidate jet, the positions of reconstructed secondary vertices and their consistency with the decay chains of such hadrons. For the working point chosen for this analysis, such jets are identified with an average efficiency of 77% in simulated $t\bar{t}$ events [84], corresponding to rejection factors of 110, 4.9 and 15 for jets originating from light quarks or gluons, charm quarks and τ leptons, respectively.

The efficiencies of the electron and muon trigger, reconstruction, identification and isolation, the jet b -tagging and Jet Vertex Tagging, and the pile-up rejection are taken into account in every simulated event by applying the respective weights that correct for deficiencies in the MC description of those efficiencies [74,75,78,81,82,84].

To avoid reconstruction of a single detected object as multiple leptons or jets, an overlap removal procedure is applied to Baseline leptons and jets. First, jet candidates are discarded if they are within $\Delta R < 0.2$ of an electron. Second, electron candidates are discarded within $\Delta R < 0.4$

of the remaining jets. Finally, muon candidates are discarded if they are within $\Delta R < 0.4$ of a remaining jet with at least three tracks of $p_T > 500$ MeV; if this jet has less than three tracks, it is discarded and the muon is kept instead.

The missing transverse momentum (whose magnitude is denoted E_T^{miss}) is defined as the negative vector sum of the transverse momenta of all identified objects (electrons, photons, muons, jets and τ -leptons) and an additional soft term. The overlap removal between baseline objects is applied before computing E_T^{miss} . The soft term is constructed from all tracks associated with the primary vertex but not with any physics object. Fully calibrated electrons, muons, photons, jets, hadronically decaying τ -leptons and charged-particle tracks are used to reconstruct E_T^{miss} [85,86].

V. EVENT SELECTION AND BACKGROUND ESTIMATION STRATEGY

The event selection is designed to be efficient for true electron + jet and muon + jet final states. For candidate signal events, $p_T > 130$ GeV is required for both the highest p_T (leading) lepton and the highest p_T jet. The invariant mass of this lepton + jet pair, m_{inv} , is required to be greater than 2.0 TeV in the signal region. A veto on subleading leptons with $p_T > 10$ GeV is applied. Subleading jets in the event are required to have $p_T < 130$ GeV. These selection requirements are summarized in Table II.

The dominant background in both channels is the W + jets process in which the W boson decays leptonically. In the electron + jet channel, the second largest background is events with nonprompt and misidentified (fake) leptons. It mostly originates from multijet production processes when one of the jets is misidentified as a lepton. In the muon channel, this background source is less than 0.5% of the total background in the signal region (SR). Its contribution is 4 times smaller than the single-top background and 10 times smaller than the total uncertainty on the sum of all the

other background contributions in the SR: it is therefore considered to be negligible in the muon + jet channel. There are also contributions from Z + jets events in which one lepton is not detected; from diboson processes in which at least one boson decays leptonically; as well as from $t\bar{t}$ and single-top-quark production, in which the W boson from the top-quark decays leptonically.

The background yields for W/Z + jets and $t\bar{t}$ processes in the SR are estimated using dedicated control regions (CRs) and confirmed in validation regions (VRs). The control (validation) regions enriched with W/Z + jets and $t\bar{t}$ backgrounds are designated as WCR (WVR), ZCR (ZVR) and TCR (TVR), respectively. They are orthogonal to each other. There are different CRs and VRs in the electron + jet and muon + jet channels. Definitions of all regions are given in Table II. The CRs/VRs are defined using m_{inv} requirements and additional selections to increase the purity of the corresponding background (last three rows in Table II). The signal contamination estimated for the CRs is less than 0.3% for the ADD signal with $M_{\text{th}} = 5$ TeV. This M_{th} value is considered since lower masses were excluded by the previous analysis at 8 TeV [12]. An additional validation region, SVR, is used to verify the agreement of the background with data in a phase space that is closer to the SR. The SVR uses the same selections as the SR but with lower m_{inv} (see Table II). The WVR and TVR are the subsets of SVR because extra requirements are applied to define WVR and TVR selections in addition to the SVR selection. The ZVR is orthogonal to SVR because two signal leptons are required in ZVR.

The multijet background for the electron channel is estimated using the data-driven *Matrix Method* described in Ref. [87]. Two parameters of the method (real and fake efficiencies, r and f) are evaluated using the MC simulated samples of the W/Z + jets background and the data samples. Events in the samples are selected with looser object requirements with respect to the Baseline selection to enrich the selected events with nonprompt electrons and nonelectron objects identified as electrons. The *Matrix*

TABLE II. Definitions of the control, validation and signal regions. Note, that “...” means that this criterion is not applied. Two same-flavor opposite-sign (SFOS) leptons satisfying the Signal selection criteria are required in the Z + jets control and validation regions, while Signal and Baseline stand for the corresponding sets of the lepton and jet selection criteria.

Event selection	WCR (WVR)	ZCR (ZVR)	TCR (TVR)	SR (SVR)
m_{inv} [TeV]	1.0–1.5 (1.5–2.0)	1.0–1.5 (1.5–2.0)	1.0–1.5 (1.5–2.0)	>2.0 (1.5–2.0)
Leading lepton, p_T [GeV]	Signal, >130	Signal, >130	Signal, >130	Signal, >130
Subleading leptons, p_T [GeV]	Baseline, <10	SFOS, >30	Baseline, <10	Baseline, <10
Leading jet, p_T [GeV]	Signal, >130	Signal, >130	Signal, >130	Signal, >130
Subleading jets, p_T [GeV]	Signal, <130	Signal, <130	Signal, <130, $N \geq 3$	Signal, <130
Number of b-tagged jets	0		≥ 2	
E_T^{miss} [GeV]	>60			
$m_{\ell^+\ell^-}$ [GeV]		70–110		

Method uses *tight* and *loose* selection. The *tight* selection corresponds to the `Signal` requirement. In contrast to *tight*, the *loose* selection uses the `Loose` identification and does not apply the isolation requirement.

The r value is the fraction of the electron candidates passing the *tight* requirements and matched to a generated electron, with respect to the electron candidates passing *loose* selection and matched also to a generated electron. The f value is the fraction of the electron candidates passing the *tight* requirements, but not matched to any generated electron (fake), with respect to the candidate electrons passing the *loose* selection and not matched to any generated electron. The r and f efficiencies and their uncertainties are estimated as a function of lepton p_T and η , and they cover all regions. The r and f efficiencies are a part of the fake/nonprompt lepton background's estimation toolset [88] that is developed using data and MC simulations and is validated in data. Estimation of the r and f uncertainties is described in Sec. VII. The number of events with fake electrons (N_{multijet}) selected with the *tight* requirement is estimated as

$$N_{\text{multijet}} = \frac{f}{r-f} (r(N_l + N_t) - N_t), \quad (2)$$

where N_t is the total number of electron candidates passing the *tight* selection in the data sample. N_l is the number of electron candidates that pass the *loose* selection and fail the *tight* requirements in the data.

All background processes (and signal sources when they are included in the fit) except the multijet are estimated using MC simulated events. The control regions are used to constrain the freely floating $W + \text{jets}$, $Z + \text{jets}$ and $t\bar{t}$ background normalization factors, which are obtained independently for the electron and muon channels. The normalizations for the multijet, diboson and single-top backgrounds are allowed to vary, but only within their uncertainty ranges.

VI. STATISTICAL ANALYSIS

A QBH signal is sought in the m_{inv} distributions in the electron + jet and muon + jet channels as well as in their combination. The statistical interpretation of the results is performed using the profile likelihood method implemented in the `HistFitter` framework [89]. The likelihood function is a product of the probability density functions of the binned m_{inv} distributions, with one for each region contributing to the fit. The number of events in each of the bins in the given regions is described using a Poisson distribution, the mean of which is the sum of the expected contributions from all background and signal sources. Systematic uncertainties described in Sec. VII are added into the fit as nuisance parameters. They are assumed to follow Gaussian distributions whose widths are determined from the size of the corresponding uncertainty. Normalization factors are free-floating parameters in the

fit. All the fit parameters are determined by maximizing the product of the Poisson probability functions and the constraints on the nuisance parameters.

The combination of the electron and muon channels was made by merging the electron and muon samples in the data and in the MC simulation. The combined channel (lepton + jet) is fitted independently from the electron and muon channels. Two types of fits are performed as detailed below.

A *model-independent* fit compares the data event yield in the SR with the SM background estimate and its uncertainties, to test for possible contribution of any non-SM signal in the SR. As a first step, a *background-only* fit is performed, where the normalization and shape fit of the backgrounds is adjusted to match the data in the three control regions simultaneously. The resulting distributions are extrapolated into the signal region to correct the expected shapes and yields of the corresponding backgrounds. The extrapolation of the adjusted distributions and nuisance parameters is also checked in the VRs by means of comparison to data and total yield of the SM background. In a second step, any non-SM signal is sought in the SR. The possible contribution of a signal is scaled by a freely floating normalization factor of the dummy signal added in the SR. The significance of a possible excess of observed events over the SM prediction is quantified by the one-sided probability, p_0 , of the background alone to fluctuate to the observed number of events or higher, by using the asymptotic formula described in Ref. [90]. The presence of a non-SM signal would manifest itself as a small p_0 value. In the absence of an excess over the SM expectation, upper limits on the cross section of any non-SM signal are estimated.

In a *model-dependent* fit, an ADD or RS1 signal is included in the SR, and its yield is scaled by a freely floating signal normalization factor. In the absence of any significant excess above the SM background prediction, limits are evaluated with the modified frequentist CL_s method [91]. The background normalization factors and nuisance parameters are determined simultaneously in the CRs and in the SR. The bin width over m_{inv} in the SR is optimized to obtain good fit performance and stability for all QBH threshold masses used in the analysis. The 2 TeV width was found to be the best bin size.

Acceptance and efficiency are estimated with the use of the simulated QBH signal event samples. Acceptance is calculated at the generation level as the fraction of events passing the signal requirements. Efficiency is the fraction of events passing the signal requirements at the reconstruction level with respect to the generation-level signal requirements. The product of acceptance and efficiency ($\text{Acc} \times \text{Eff}$) of the signal selection does not depend on the QBH threshold mass within their uncertainties. The $\text{Acc} \times \text{Eff}$ is also consistent for both models (ADD and RS1). The average values of $\text{Acc} \times \text{Eff}$ are equal to $(66.5 \pm 0.4)\%$ and $(67.1 \pm 0.4)\%$ in the electron and muon channels, respectively.

The suppression of the additional jet activity in the event due to the vetoing of subleading jets with $p_T > 130$ GeV leads to a better separation between the signal and SM background processes. However, the constraint distorts the acceptance and efficiency of the signal extraction from the background, since the QBH signal is calculated at LO + PS accuracy in QCD, while the largest SM backgrounds, $V + \text{jets}$, are generated with NLO + PS precision. Thus, the comparison of signal with background may be distorted in the fit, leading to an over-optimistic estimate of upper limits on $\sigma \times Br$. The effect of the higher order QCD radiation in the QBH production yield is evaluated as a correction factor, R_c . The R_c is obtained using the $W/Z + \text{jets}$ samples, since the events have a color structure in the final state similar to that of the signal and are generated at higher order accuracy. Hence, the R_c quantifies the overestimate in signal acceptance and efficiency due to use of the veto on the high- p_T subleading jets at LO MC generated events.

The R_c is defined as the ratio of the number of events passing the signal selection without and with the requirement on the subleading jet activity (see Table II). The ratios are calculated separately for $W + \text{jets}$ and $Z + \text{jets}$ events, and the average of the two is used as the R_c correction factor. The maximal difference between corrections obtained with the $W + \text{jets}$ and $Z + \text{jets}$ samples is used as the systematic uncertainty on the R_c factor. Statistical uncertainties in the $W/Z + \text{jets}$ samples are also included in the R_c total uncertainty. The uncertainty on R_c was added to the total systematic uncertainty in the fit. The QCD correction for the electron + jet and muon + jet final-states combination is calculated as the weighted average. The R_c correction factors in the electron and muon channels and their combination are given in Eq. (3), respectively:

$$\begin{aligned} \langle R_c \rangle^{\text{ele}} &= 0.36 \pm 0.02, & \langle R_c \rangle^{\text{muo}} &= 0.39 \pm 0.04, \\ \langle R_c \rangle^{\text{comb}} &= 0.37 \pm 0.02. \end{aligned} \quad (3)$$

The R_c factors are consistent between the electron, muon and combined channels and are used to correct the signal MC $\text{Acc} \times \text{Eff}$ in the limit setting procedure.

VII. SYSTEMATIC UNCERTAINTIES

Systematic uncertainties are evaluated for all signal and background predictions and include experimental uncertainties on detector measurements as well as modeling uncertainties and the effect of limited statistics of MC simulation. The systematic uncertainties of all backgrounds are extrapolated from the control regions into the validation and signal regions in the background-only fit. The background uncertainties are practically the same in all types of fit. The expected QBH signal and its uncertainties are estimated for the ADD and RS1 models in the

TABLE III. The relative systematic uncertainties (in %) on the SM background in the SR are estimated in the background-only fit; and systematic uncertainties on the ADD signal are estimated for the QBH with $M_{\text{th}} = 6.0$ TeV in the model-dependent fit. Lepton modeling combines all the types of experimental uncertainties for the electrons or muons. All the uncertainties shown are obtained independently for the electron and muon channels. The relative statistical errors on the data (in %) are also shown.

Source	Electron + jet		Muon + jet	
	Background	Signal	Background	Signal
JER	2.4	1.9	2.4	1.6
JES	0.7	0.4	0.6	0.5
Lepton modeling	2.8	0.6	3.6	1.7
Pileup	0.7	0.6	0.8	1.0
Luminosity	0.5	0.7	0.5	0.7
$W + \text{jets}$ normalization	1.1		1.1	
$W + \text{jets}$ modeling	0.5		0.6	
$Z + \text{jets}$ normalization	0.3		0.3	
$Z + \text{jets}$ modeling	0.3		0.3	
$t\bar{t}$ normalization	0.2		0.4	
MC statistics	1.6	0.6	1.5	0.7
Multijet estimation	1.4			
Total uncertainty	4.6	2.4	5.1	2.7
Statistical errors of data	2.1		2.7	

model-dependent fit. The relative systematic uncertainties for the SM background and a representative signal (ADD, $M_{\text{th}} = 6.0$ TeV) in the SR are represented in Table III. The resulting uncertainty in the total background differs from the sum in quadrature of the single sources because of correlations.

Experimental uncertainties reflect the accuracy of the experimental measurements of jets and leptons. The jet energy scale (JES) and resolution (JER) uncertainties are derived as a function of the p_T and η of the jet. They are determined using a combination of data and simulation, through measurements of the jet p_T balance in dijet, $Z + \text{jets}$ and $\gamma + \text{jets}$ events [80]. The uncertainties in scale and resolution of the electron energy [74] and muon momentum [75] are propagated to the measured event yield. Systematic uncertainties in the measurements of the electron [33,74] and muon [75] identification, reconstruction, isolation, and triggering efficiencies as well as in the pile-up jet identification using the jet vertex tagger algorithm [82] are also propagated to the measured m_{inv} distributions.

The uncertainty in the m_{inv} spectrum due to pileup is estimated by varying the average number of pile-up events in the simulation to account for the differences between the values of the measured and predicted total inelastic cross section used in the pile-up simulation [92]. The impact of the luminosity uncertainty on the SM background is

estimated by varying the integrated luminosity combined over 2015–2018 within its uncertainty of 0.83% [35].

Modeling uncertainties on the $W/Z + \text{jets}$ backgrounds are calculated as follows. The PDF uncertainties propagated to the m_{inv} distribution are estimated using the nominal PDF set and a set of 100 PDF replicas for NNPDF3.0NNLO [42].

The impact of the $\alpha_s(m_Z)$ uncertainty on the background is estimated by varying $\Delta\alpha_s(m_Z) = \pm 0.002$. The impact of missing higher order calculations is evaluated using seven-point variations of the factorization and renormalization scales in the cross section calculations. The scales are independently varied upward and downward by a factor

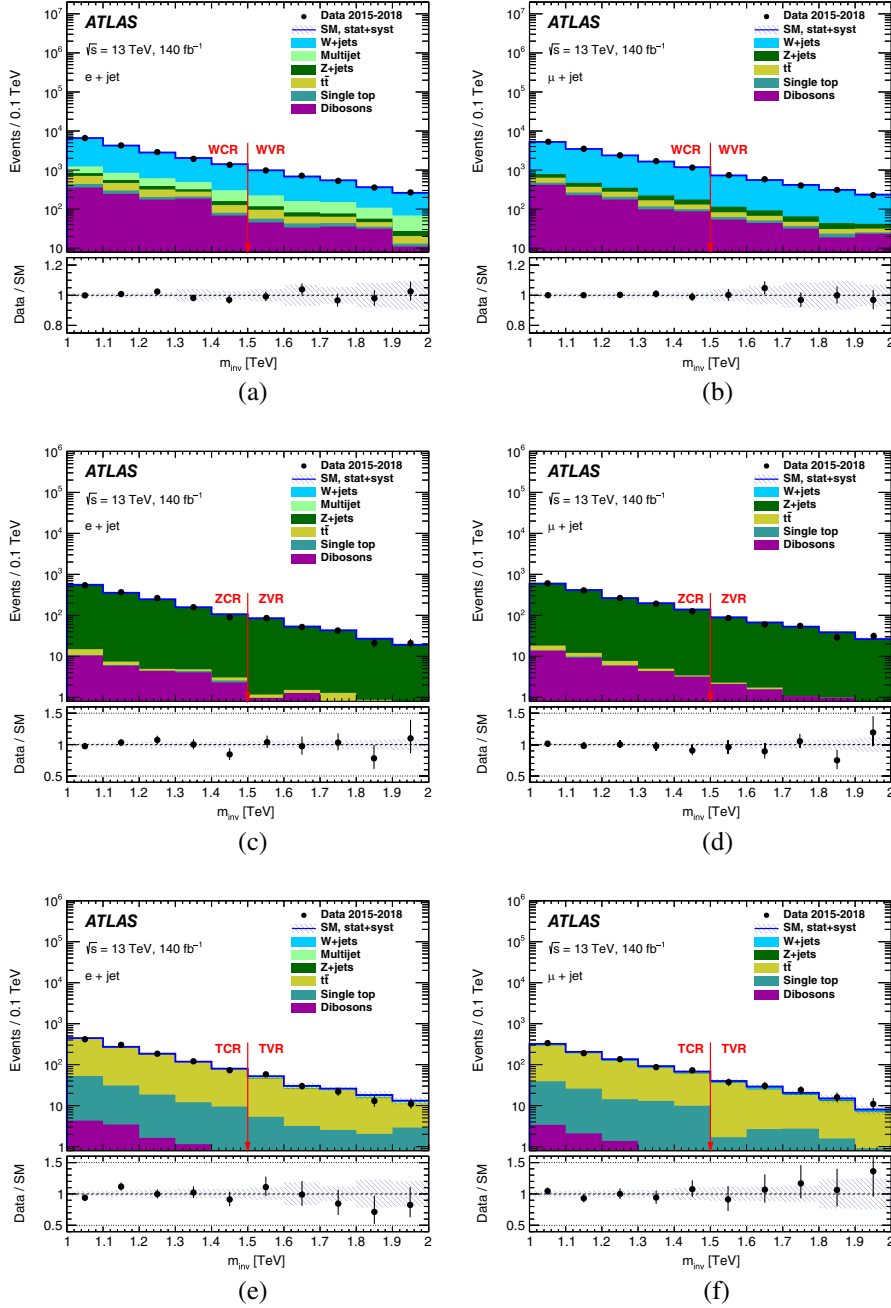


FIG. 1. The distributions of events over the invariant mass of the leading lepton and the leading jet are shown after the *background-only* fit. The data (points with error bars) and SM backgrounds (solid histograms) are shown in (a), (c), and (e) for the electron + jet channel and in (b), (d), and (f) for the muon + jet channel. The normalizations extracted from the fit in the CRs are applied in the full m_{inv} range. (a),(b) The WCR and WVR. (c),(d) The ZCR and ZVR. (e),(f) The TCR and TVR. The lower panels show the ratio of the number of events observed in the data to the fitted total background. The hatched bands represent the total relative uncertainty in the background estimate.

TABLE IV. The observed number of data events, the fitted background events in the SVR and the SR for the *background-only* fit and the number of background events expected from the MC background samples in the electron + jet and muon + jet channels. The errors shown for the “Expected events” are statistical and systematic uncertainties summed in quadrature.

	SVR electron + jet	SVR muon + jet	SR electron + jet	SR muon + jet
Observed data	9053	5504	2319	1359
Fitted events	8900 ± 320	5380 ± 200	2290 ± 110	1386 ± 70
W + jets	5590 ± 270	4190 ± 200	1290 ± 70	1087 ± 54
Multijet	1670 ± 200		570 ± 47	
Z + jets	646 ± 73	439 ± 27	199 ± 17	131 ± 13
$t\bar{t}$	527 ± 10	351 ± 7	109 ± 5	69 ± 5
Single top	143 ± 7	112 ± 5	31 ± 2	28 ± 2
Dibosons	335 ± 22	289 ± 14	94 ± 9	72 ± 8
Expected events	9390 ± 340	5260 ± 220	2647 ± 94	1303 ± 55
W + jets	6090 ± 270	4080 ± 210	1654 ± 65	1016 ± 48
Multijet	1690 ± 210		577 ± 38	
Z + jets	598 ± 85	408 ± 23	186 ± 18	122 ± 12
$t\bar{t}$	546 ± 14	366 ± 7	109 ± 6	71 ± 5
Single top	141 ± 7	104 ± 4	29 ± 2	28 ± 2
Dibosons	327 ± 23	298 ± 12	92 ± 10	66 ± 8

of 2, excluding simultaneous variations in opposite directions. The envelope of the resulting variations as a function of m_{inv} is taken as the size of the associated systematic uncertainty. All aforementioned modeling uncertainties are combined in quadrature and represented in Table III as “ W/Z + jets modeling.” Total modeling (theoretical) uncertainties are not estimated for the $t\bar{t}$, single-top and diboson samples because they are small backgrounds. The uncertainties in the normalization of the W/Z + jets and $t\bar{t}$ backgrounds from the fitting procedure are shown in Table III as well as uncertainties from the limited MC statistics of the background simulated samples.

The uncertainties in the multijet background are related to the estimate of the f and r parameters (Δf and Δr) as well as to statistical errors in the total number N_t of *tight* electron candidates (ΔN_t) and in the total number N_l of *loose* electron candidates (ΔN_l). The Δf and Δr uncertainties are estimated for different ($\eta - p_T$) regions by varying the requirements used in the event selection [87]. All these uncertainties are combined in quadrature and reported in Table III.

Systematic uncertainties described in this section are added into the fit as nuisance parameters where they can be pulled and constrained. After the fit all systematic uncertainties are pulled by less than 0.7 of a standard deviation. The errors of nuisance parameters are constrained within $\pm 0.5\sigma$ in comparison with their initial values.

VIII. RESULTS

In the *background-only* fit, the normalization factors of the W + jets, Z + jets and $t\bar{t}$ background processes are consistent with unity within uncertainties. Differences of normalization factors from unity are $\leq 5\%$ in all cases. The

m_{inv} distributions of events in the WCR, ZCR, TCR and corresponding validation regions after the *background-only* fit are shown in Fig. 1. There is good agreement between the data and the SM background in all CRs and VRs.

The comparison of the post-fit background yields with the data in the SVR and SR is represented in Table IV. The pre-fit background yields expected in the MC are shown in the bottom part of Table IV. There is agreement between the data (“Observed data”) and the total SM background (“Fitted events”) within 1σ in all regions. The errors include both statistical and systematic uncertainties.

The difference between expected and fitted yields of W + jet background in the electron channel in Table IV is $\sim 10\%$ in SVR and $\sim 20\%$ in SR, with the W + jet normalization factor close to unity (1.01 ± 0.02), since the pre-fit W + jet background in the electron channel has a visible slope relative to data. The W + jet distribution is fitted to data in CRs where both the slope and the normalization are adjusted. The slope elimination is a result of simultaneous pulls of several nuisance parameters. The main contributors are five parameters that tune the W + jet yields in the 5-bin WCR in the likelihood fit. The total uncertainty includes statistical errors, uncertainties on normalization and slope elimination, and nuisance parameters related to objects, detector, and modeling.

The m_{inv} distributions after the *background-only* fit shown in Fig. 2 have good agreement between the data and the SM background in the SR in both the electron + jet and the muon + jet channels. The differences between the data and background are within 1σ . The highest invariant mass of a lepton + jet pair reconstructed in the electron (muon) channel is 4.74 TeV (4.96 TeV).

The *model-independent* fit is performed simultaneously in the WCR, ZCR, TCR and a single-bin SR to test for a

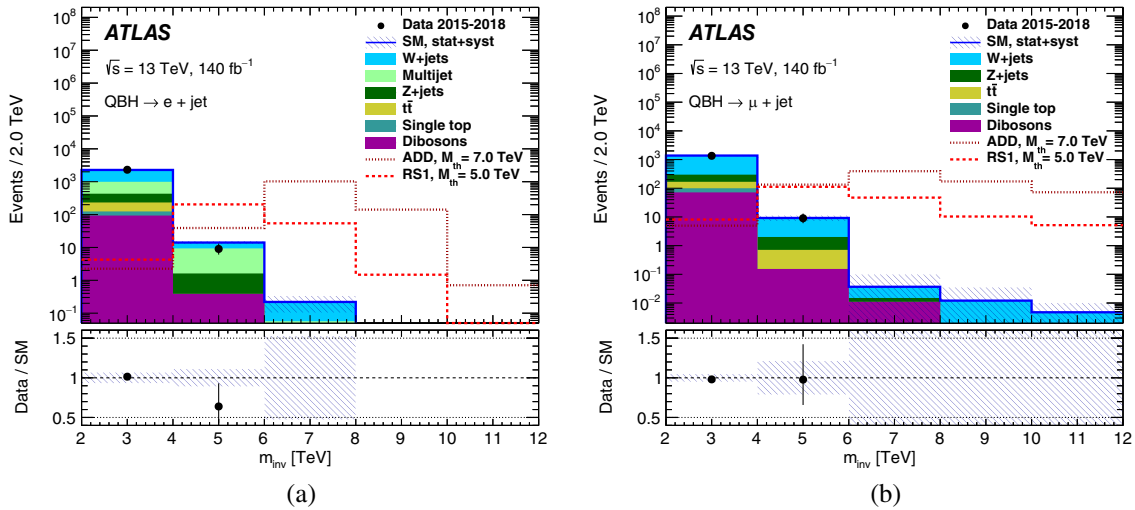


FIG. 2. The distributions of events over the invariant mass of the leading lepton and the leading jet in the SR for data (points with error bars) and for SM backgrounds (solid histograms) after the *background-only* fit are shown in (a) the electron + jet and (b) the muon + jet channels. The normalizations extracted from the fit in the CRs are applied in the full m_{inv} range including the SR. The sum of the systematic uncertainties and the statistical errors due to the limited size of the fitted MC samples is shown by the hatched area. The lower panels show the ratios of the number of events observed in the data to the fitted total background. The hatched area represents the total relative uncertainty in the background estimate. Two examples of QBH signals normalized to the predicted cross section are overlaid.

non-SM signal contribution. The possible contribution of signal events is scaled by a freely floating signal normalization factor. No significant excess above the SM background prediction is observed in either of the channels. The *model-independent* upper limit on the cross section times branching fraction ($\sigma \times Br$) is estimated at 95% confidence level (CL) for the production of a non-SM signal.

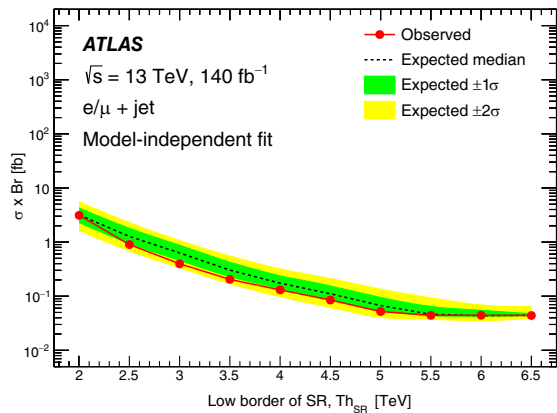


FIG. 3. The 95% CL *model-independent* upper limits on $\sigma \times Br$ for the non-SM signal production with decay into lepton + jet (combined channel). The limits take into account statistical and systematic uncertainties. Circles along the solid red line indicate the lower border of the SR (threshold of SR, Th_{SR}), above which the observed limit is computed. The expected limits are shown by the dashed line. The $\pm 1\sigma$ and $\pm 2\sigma$ bands of expected limits are shown in green and yellow, respectively. The limits are obtained with pseudoexperiments.

Figure 3 shows the upper limits on the $\sigma \times Br$ (circles along the solid red line) integrated above the lower threshold of the SR (events with $m_{\text{inv}} > Th_{\text{SR}}$) for the lepton + jet channel (combined channel of electron + jet and muon + jet).

In the *model-dependent* fit, the 5-bin m_{inv} distributions of signal and backgrounds in the SR are fitted simultaneously with background in three CRs. The number of ADD (RS1) signal events is scaled by a freely floating signal normalization factor. The background normalization factors are also determined simultaneously in the fit in the CRs, and they are consistent with those of the *background-only* fit. There is no evidence of a QBH signal at any M_{th} in both models. Figure 4 shows the 95% CL upper limit on the cross section times branching fraction³ ($\sigma \times Br$) as a function of M_{th} for the combined lepton + jet channel for the production of a QBH in the ADD and RS1 models. The limits are obtained using pseudoexperiments with a spacing of 0.5 TeV in M_{th} , and they are linearly interpolated between the points.

The lower limits on M_{th} for ADD and RS1, upper limits on $\sigma \times Br$ at the M_{th} mass point limits and model-independent upper limits on $\sigma(m_{\text{inv}} > 5 \text{ TeV}) \times Br$ are shown in Table V. Accounting for QCD radiation effects in the QBH production using the R_c correction factor leads to more stringent limit estimates than without it. Future QBH lepton + jet analyses have the potential to explore higher

³There are six QBH states that can decay to lepton + jet. As each state has a different production cross section and branching fraction, the limits set an effective limit which is a sum over all possible QBH states.

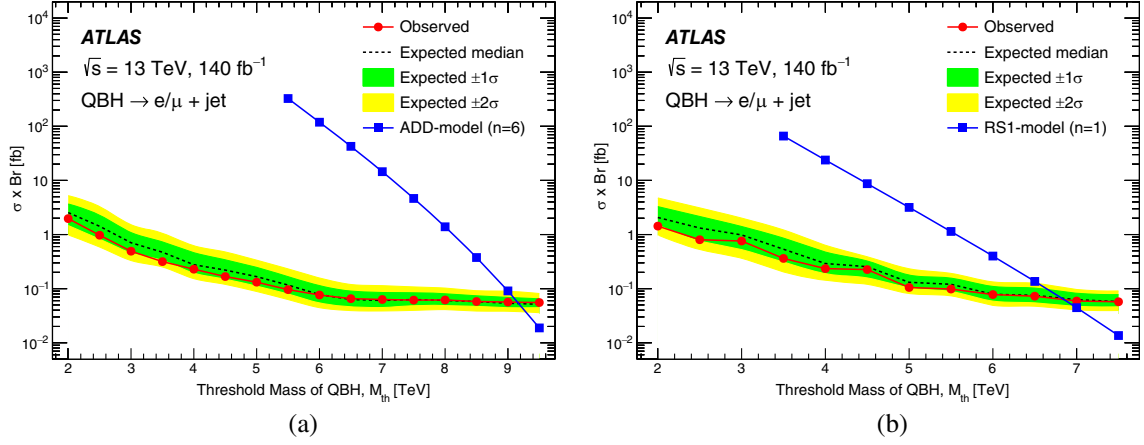


FIG. 4. The combined 95% CL upper limits on $\sigma \times Br$ as a function of M_{th} for QBH production at $M_{th} = M_D$ with decay into lepton + jet for (a) ADD (extra dimensions $n = 6$) and (b) RS1 (extra dimensions $n = 1$). The limits take into account statistical and systematic uncertainties. Circles along the solid red line indicate the mass M_{th} of the signal where the observed limit is computed. The expected limits are shown by the dashed line. The $\pm 1\sigma$ and $\pm 2\sigma$ bands are shown in green and yellow, respectively. The theoretically predicted $\sigma \times Br$ for the QBH production and decay is shown as the solid blue curve with squares. The limits are obtained with pseudoexperiments.

TABLE V. The lower limits on M_{th} and the upper limits on $\sigma \times Br$ at these mass points for QBHs decaying to a lepton and jet in the ADD and RS1 models. The model-independent upper limits on $\sigma \times Br$ are shown at $m_{inv} > 5$ TeV.

Channel	ADD	ADD	RS1	RS1	Model-independent
	$\sigma \times Br$ [fb]	M_{th} [TeV]	$\sigma \times Br$ [fb]	M_{th} [TeV]	$\sigma(m_{inv} > 5 \text{ TeV}) \times Br$ [fb]
Electron + jet	0.091	9.0	0.099	6.6	0.095
Muon + jet	0.083	9.0	0.087	6.7	0.084
Combined	0.056	9.2	0.061	6.8	0.052

QBH mass ranges and lower QBH production cross section values once hard QCD radiation effects are included in the QBH event generation model.

IX. CONCLUSION

The ATLAS detector at the LHC has been used to search for new phenomena in the lepton + jet invariant mass spectrum. The search is performed with 140 fb^{-1} of proton-proton collision data at $\sqrt{s} = 13 \text{ TeV}$, recorded during 2015–2018. The observed invariant mass spectrum of lepton + jet pairs is consistent with SM expectations. Upper exclusion limits are set on the cross section times branching fraction for quantum black holes decaying to a lepton and a quark in a search region with invariant mass above 2.0 TeV. The resulting lower mass threshold limits in the ADD (RS1) models with six (one) extra dimensions at the 95% CL are 9.2 (6.8) TeV. The obtained limits show a factor of 3.5 improvement with respect to the previous model-independent upper limit on $\sigma \times Br$ [12]. The obtained limit on the QBH threshold mass for the ADD model is 3.9 TeV higher compared to the previous ATLAS result in this channel at 8 TeV [12]. The obtained limit on

the QBH M_{th} for the RS1 model is determined for the first time in the lepton + jet decay mode.

ACKNOWLEDGMENTS

We thank CERN for the very successful operation of the LHC, as well as the support staff from our institutions without whom ATLAS could not be operated efficiently. We acknowledge the support of ANPCyT, Argentina; YerPhI, Armenia; ARC, Australia; BMWFW and FWF, Austria; ANAS, Azerbaijan; CNPq and FAPESP, Brazil; NSERC, NRC and CFI, Canada; CERN; ANID, Chile; CAS, MOST and NSFC, China; Minciencias, Colombia; MEYS CR, Czech Republic; DNRF and DNSRC, Denmark; IN2P3-CNRS and CEA-DRF/IRFU, France; SRNSFG, Georgia; BMBF, HGF and MPG, Germany; GSRI, Greece; RGC and Hong Kong SAR, China; ISF and Benozio Center, Israel; INFN, Italy; MEXT and JSPS, Japan; CNRST, Morocco; NWO, Netherlands; RCN, Norway; MEiN, Poland; FCT, Portugal; MNE/IFA, Romania; MESTD, Serbia; MSSR, Slovakia; ARRS and MIZŠ, Slovenia; DSI/NRF, South Africa; MICINN, Spain; SRC and Wallenberg Foundation, Sweden; SERI, SNSF

and Cantons of Bern and Geneva, Switzerland; MOST, Taiwan; TENMAK, Türkiye; STFC, United Kingdom; DOE and NSF, United States of America. In addition, individual groups and members have received support from BCKDF, CANARIE, Compute Canada and CRC, Canada; PRIMUS 21/SCI/017 and UNCE SCI/013, Czech Republic; COST, ERC, ERDF, Horizon 2020, ICSC-NextGenerationEU and Marie Skłodowska-Curie Actions, European Union; Investissements d’Avenir Labex, Investissements d’Avenir IDEX and ANR, France; DFG and AvH Foundation, Germany; Herakleitos, Thales and Aristeia programs cofinanced by EU-ESF and the Greek NSRF, Greece; BSF-NSF and MINERVA, Israel; Norwegian Financial Mechanism 2014-2021, Norway; NCN and NAWA, Poland; La Caixa

Banking Foundation, CERCA Programme Generalitat de Catalunya and PROMETEO and GenT Programmes Generalitat Valenciana, Spain; Göran Gustafssons Stiftelse, Sweden; The Royal Society and Leverhulme Trust, United Kingdom. The crucial computing support from all WLCG partners is acknowledged gratefully, in particular from CERN, the ATLAS Tier-1 facilities at TRIUMF (Canada), NDGF (Denmark, Norway, Sweden), CC-IN2P3 (France), KIT/GridKA (Germany), INFN-CNAF (Italy), NL-T1 (Netherlands), PIC (Spain), ASGC (Taiwan), RAL (UK) and BNL (USA), the Tier-2 facilities worldwide and large non-WLCG resource providers. Major contributors of computing resources are listed in Ref. [93].

-
- [1] N. Arkani-Hamed, S. Dimopoulos, and G. Dvali, The hierarchy problem and new dimensions at a millimeter, *Phys. Lett. B* **429**, 263 (1998).
- [2] I. Antoniadis, N. Arkani-Hamed, S. Dimopoulos, and G. Dvali, New dimensions at a millimeter to a Fermi and superstrings at a TeV, *Phys. Lett. B* **436**, 257 (1998).
- [3] L. Randall and R. Sundrum, Large mass hierarchy from a small extra dimension, *Phys. Rev. Lett.* **83**, 3370 (1999).
- [4] P. Meade and L. Randall, Black holes and quantum gravity at the LHC, *J. High Energy Phys.* **05** (2008) 003.
- [5] X. Calmet, W. Gong, and S. D. H. Hsu, Colorful quantum black holes at the LHC, *Phys. Lett. B* **668**, 20 (2008).
- [6] D. M. Gingrich, Quantum black holes with charge, color and spin at the LHC, *J. Phys. G* **37**, 105008 (2010).
- [7] L. A. Anchordoqui, J. L. Feng, H. Goldberg, and A. D. Shapere, Black holes from cosmic rays: Probes of extra dimensions and new limits on TeV-scale gravity, *Phys. Rev. D* **65**, 124027 (2002).
- [8] ATLAS Collaboration, Search for strong gravity in multijet final states produced in pp collisions at $\sqrt{s} = 13$ TeV using the ATLAS detector at the LHC, *J. High Energy Phys.* **03** (2016) 026.
- [9] ATLAS Collaboration, Search for heavy particles decaying into top-quark pairs using lepton-plus-jets events in proton–proton collisions at $\sqrt{s} = 13$ TeV with the ATLAS detector, *Eur. Phys. J. C* **78**, 565 (2018).
- [10] CMS Collaboration, Search for black holes and other new phenomena in high-multiplicity final states in proton–proton collisions at $\sqrt{s} = 13$ TeV, *Phys. Lett. B* **774**, 279 (2017).
- [11] CMS Collaboration, Search for black holes and sphalerons in high-multiplicity final states in proton–proton collisions at $\sqrt{s} = 13$ TeV, *J. High Energy Phys.* **11** (2018) 042.
- [12] ATLAS Collaboration, Search for quantum black hole production in high-invariant-mass lepton + jet final states using pp collisions at $\sqrt{s} = 8$ TeV and the ATLAS detector, *Phys. Rev. Lett.* **112**, 091804 (2014).
- [13] ATLAS Collaboration, A search for new physics in dijet mass and angular distributions in pp collisions at $\sqrt{s} = 7$ TeV measured with the ATLAS detector, *New J. Phys.* **13**, 053044 (2011).
- [14] ATLAS Collaboration, ATLAS search for new phenomena in dijet mass and angular distributions using pp collisions at $\sqrt{s} = 7$ TeV, *J. High Energy Phys.* **01** (2013) 029.
- [15] CMS Collaboration, Search for narrow resonances and quantum black holes in inclusive and b -tagged dijet mass spectra from pp collisions at $\sqrt{s} = 7$ TeV, *J. High Energy Phys.* **01** (2013) 013.
- [16] ATLAS Collaboration, Search for new phenomena in photon + jet events collected in proton–proton collisions at $\sqrt{s} = 8$ TeV with the ATLAS detector, *Phys. Lett. B* **728**, 562 (2014).
- [17] ATLAS Collaboration, Search for high-mass dilepton resonances in pp collisions at $\sqrt{s} = 8$ TeV with the ATLAS detector, *Phys. Rev. D* **90**, 052005 (2014).
- [18] ATLAS Collaboration, Search for new phenomena in the dijet mass distribution using pp collision data at $\sqrt{s} = 8$ TeV with the ATLAS detector, *Phys. Rev. D* **91**, 052007 (2015).
- [19] CMS Collaboration, Search for resonances and quantum black holes using dijet mass spectra in proton–proton collisions at $\sqrt{s} = 8$ TeV, *Phys. Rev. D* **91**, 052009 (2015).
- [20] ATLAS Collaboration, Search for new phenomena in final states with an energetic jet and large missing transverse momentum in pp collisions at $\sqrt{s} = 8$ TeV with the ATLAS detector, *Eur. Phys. J. C* **75**, 299 (2015); **75**, 408(E) (2015).
- [21] ATLAS Collaboration, Search for new phenomena in dijet mass and angular distributions from pp collisions at $\sqrt{s} = 13$ TeV with the ATLAS detector, *Phys. Lett. B* **754**, 302 (2016).
- [22] ATLAS Collaboration, Search for new phenomena in different-flavour high-mass dilepton final states in pp collisions at $\sqrt{s} = 13$ TeV with the ATLAS detector, *Eur. Phys. J. C* **76**, 541 (2016).

- [23] CMS Collaboration, Search for new physics with dijet angular distributions in proton–proton collisions at $\sqrt{s} = 13$ TeV, *J. High Energy Phys.* **07** (2017) 013.
- [24] CMS Collaboration, Search for lepton-flavor violating decays of heavy resonances and quantum black holes to $e\mu$ final states in proton–proton collisions at $\sqrt{s} = 13$ TeV, *J. High Energy Phys.* **04** (2018) 073.
- [25] ATLAS Collaboration, Search for new resonances in mass distributions of jet pairs using 139 fb^{-1} of pp collisions at $\sqrt{s} = 13$ TeV with the ATLAS detector, *J. High Energy Phys.* **03** (2020) 145.
- [26] CMS Collaboration, Search for heavy resonances and quantum black holes in $e\mu$, $e\tau$, and $\mu\tau$ final states in proton–proton collisions at $\sqrt{s} = 13$ TeV, *J. High Energy Phys.* **05** (2023) 227.
- [27] ATLAS Collaboration, Search for lepton-flavour violation in high-mass dilepton final states using 139 fb^{-1} of pp collisions at $\sqrt{s} = 13$ TeV with the ATLAS detector, *J. High Energy Phys.* **10** (2023) 082.
- [28] ATLAS Collaboration, The ATLAS experiment at the CERN Large Hadron Collider, *J. Instrum.* **3**, S08003 (2008).
- [29] B. Abbott *et al.*, Production and integration of the ATLAS insertable B-layer, *J. Instrum.* **13**, T05008 (2018).
- [30] ATLAS Collaboration, Performance of the ATLAS trigger system in 2015, *Eur. Phys. J. C* **77**, 317 (2017).
- [31] ATLAS Collaboration, The ATLAS Collaboration software and firmware, Report No. ATL-SOFT-PUB-2021-001, 2021, <https://cds.cern.ch/record/2767187>.
- [32] ATLAS Collaboration, ATLAS data quality operations and performance for 2015–2018 data-taking, *J. Instrum.* **15**, P04003 (2020).
- [33] ATLAS Collaboration, Performance of electron and photon triggers in ATLAS during LHC Run 2, *Eur. Phys. J. C* **80**, 47 (2020).
- [34] ATLAS Collaboration, Performance of the ATLAS muon triggers in Run 2, *J. Instrum.* **15**, P09015 (2020).
- [35] ATLAS Collaboration, Luminosity determination in pp collisions at $\sqrt{s} = 13$ TeV using the ATLAS detector at the LHC, *Eur. Phys. J. C* **83**, 982 (2023).
- [36] G. Avoni *et al.*, The new LUCID-2 detector for luminosity measurement and monitoring in ATLAS, *J. Instrum.* **13**, P07017 (2018).
- [37] ATLAS Collaboration, Multi-boson simulation for 13 TeV ATLAS analyses, Report No. ATL-PHYS-PUB-2017-005, 2017, <https://cds.cern.ch/record/2261933>.
- [38] ATLAS Collaboration, ATLAS simulation of boson plus jets processes in Run 2, Report No. ATL-PHYS-PUB-2017-006, 2017, <https://cds.cern.ch/record/2261937>.
- [39] E. Bothmann *et al.*, Event generation with Sherpa 2.2, *SciPost Phys.* **7**, 034 (2019).
- [40] T. Gleisberg and S. Höche, Comix, a new matrix element generator, *J. High Energy Phys.* **12** (2008) 039.
- [41] S. Schumann and F. Krauss, A parton shower algorithm based on Catani–Seymour dipole factorisation, *J. High Energy Phys.* **03** (2008) 038.
- [42] R. D. Ball *et al.* (The NNPDF Collaboration), Parton distributions for the LHC run II, *J. High Energy Phys.* **04** (2015) 040.
- [43] S. Höche, F. Krauss, M. Schönherr, and F. Siegert, A critical appraisal of NLO + PS matching methods, *J. High Energy Phys.* **09** (2012) 049.
- [44] S. Höche, F. Krauss, M. Schönherr, and F. Siegert, QCD matrix elements + parton showers. The NLO case, *J. High Energy Phys.* **04** (2013) 027.
- [45] S. Catani, F. Krauss, B. R. Webber, and R. Kuhn, QCD matrix elements + parton showers, *J. High Energy Phys.* **11** (2001) 063.
- [46] S. Höche, F. Krauss, S. Schumann, and F. Siegert, QCD matrix elements and truncated showers, *J. High Energy Phys.* **05** (2009) 053.
- [47] F. Cascioli, P. Maierhöfer, and S. Pozzorini, Scattering amplitudes with open loops, *Phys. Rev. Lett.* **108**, 111601 (2012).
- [48] A. Denner, S. Dittmaier, and L. Hofer, Collier: A Fortran-based complex one-loop library in extended regularizations, *Comput. Phys. Commun.* **212**, 220 (2017).
- [49] C. Anastasiou, L. J. Dixon, K. Melnikov, and F. Petriello, High precision QCD at hadron colliders: Electroweak gauge boson rapidity distributions at next-to-next-to leading order, *Phys. Rev. D* **69**, 094008 (2004).
- [50] M. Grazzini, S. Kallweit, and D. Rathlev, ZZ production at the LHC: Fiducial cross sections and distributions in NNLO QCD, *Phys. Lett. B* **750**, 407 (2015).
- [51] S. Frixione, P. Nason, and G. Ridolfi, A positive-weight next-to-leading-order Monte Carlo for heavy flavour hadroproduction, *J. High Energy Phys.* **09** (2007) 126.
- [52] E. Re, Single-top Wt-channel production matched with parton showers using the POWHEG method, *Eur. Phys. J. C* **71**, 1547 (2011).
- [53] S. Alioli, P. Nason, C. Oleari, and E. Re, NLO single-top production matched with shower in POWHEG: s - and t -channel contributions, *J. High Energy Phys.* **09** (2009) 111.
- [54] P. Nason, A new method for combining NLO QCD with shower Monte Carlo algorithms, *J. High Energy Phys.* **11** (2004) 040.
- [55] S. Frixione, P. Nason, and C. Oleari, Matching NLO QCD computations with parton shower simulations: The POWHEG method, *J. High Energy Phys.* **11** (2007) 070.
- [56] S. Alioli, P. Nason, C. Oleari, and E. Re, A general framework for implementing NLO calculations in shower Monte Carlo programs: The POWHEG BOX, *J. High Energy Phys.* **06** (2010) 043.
- [57] R. Frederix, E. Re, and P. Torrielli, Single-top t-channel hadroproduction in the four-flavour scheme with POWHEG and aMC@NLO, *J. High Energy Phys.* **09** (2012) 130.
- [58] T. Sjöstrand, S. Ask, J. R. Christiansen, R. Corke, N. Desai, P. Ilten, S. Mrenna, S. Prestel, C. O. Rasmussen, and P. Z. Skands, An introduction to PYTHIA 8.2, *Comput. Phys. Commun.* **191**, 159 (2015).
- [59] ATLAS Collaboration, ATLAS PYTHIA 8 tunes to 7 TeV data, Report No. ATL-PHYS-PUB-2014-021, 2014, <https://cds.cern.ch/record/1966419>.
- [60] R. D. Ball *et al.* (NNPDF Collaboration), Parton distributions with LHC data, *Nucl. Phys.* **B867**, 244 (2013).
- [61] ATLAS Collaboration, Studies on top-quark Monte Carlo modelling for Top2016, Report No. ATL-PHYS-PUB-2016-020, 2016, <https://cds.cern.ch/record/2216168>.

- [62] M. Czakon and A. Mitov, `Top++`: A program for the calculation of the top-pair cross section at hadron colliders, *Comput. Phys. Commun.* **185**, 2930 (2014).
- [63] M. Aliev, H. Lacker, U. Langenfeld, S. Moch, P. Uwer, and M. Wiedermann, HATHOR: Hadronic top and heavy quarks cross section calculator, *Comput. Phys. Commun.* **182**, 1034 (2011).
- [64] P. Kant, O.M. Kind, T. Kintscher, T. Lohse, T. Martini, S. Mölbitz, P. Rieck, and P. Uwer, HatHor for single top-quark production: Updated predictions and uncertainty estimates for single top-quark production in hadronic collisions, *Comput. Phys. Commun.* **191**, 74 (2015).
- [65] P. Artoisenet, R. Frederix, O. Mattelaer, and R. Rietkerk, Automatic spin-entangled decays of heavy resonances in Monte Carlo simulations, *J. High Energy Phys.* **03** (2013) 015.
- [66] D. J. Lange, The EvtGen particle decay simulation package, *Nucl. Instrum. Methods Phys. Res., Sect. A* **462**, 152 (2001).
- [67] D.M. Gingrich, Monte Carlo event generator for black hole production and decay in proton-proton collisions—QBH version 1.02, *Comput. Phys. Commun.* **181**, 1917 (2010).
- [68] D. Stump, J. Huston, J. Pumplin, W.-K. Tung, H.-L. Lai, S. Kuhlmann, and J. F. Owens, Inclusive jet production, parton distributions, and the search for new physics, *J. High Energy Phys.* **10** (2003) 046.
- [69] ATLAS Collaboration, The PYTHIA 8 A3 tune description of ATLAS minimum bias and inelastic measurements incorporating the Donnachie–Landshoff diffractive model, Report No. ATL-PHYS-PUB-2016-017, 2016, <https://cds.cern.ch/record/2206965>.
- [70] ATLAS Collaboration, The ATLAS simulation infrastructure, *Eur. Phys. J. C* **70**, 823 (2010).
- [71] S. Agostinelli *et al.*, GEANT4—A simulation toolkit, *Nucl. Instrum. Methods Phys. Res., Sect. A* **506**, 250 (2003).
- [72] ATLAS Collaboration, The simulation principle and performance of the ATLAS fast calorimeter simulation FastCaloSim, Report No. ATL-PHYS-PUB-2010-013, 2010, <https://cds.cern.ch/record/1300517>.
- [73] ATLAS Collaboration, Vertex reconstruction performance of the ATLAS detector at $\sqrt{s} = 13$ TeV, Report No. ATL-PHYS-PUB-2015-026, 2015, <https://cds.cern.ch/record/2037717>.
- [74] ATLAS Collaboration, Electron and photon performance measurements with the ATLAS detector using the 2015–2017 LHC proton–proton collision data, *J. Instrum.* **14**, P12006 (2019).
- [75] ATLAS Collaboration, Muon reconstruction performance of the ATLAS detector in proton–proton collision data at $\sqrt{s} = 13$ TeV, *Eur. Phys. J. C* **76**, 292 (2016).
- [76] M. Cacciari, G. P. Salam, and G. Soyez, The anti- k_r jet clustering algorithm, *J. High Energy Phys.* **04** (2008) 063.
- [77] M. Cacciari, G. P. Salam, and G. Soyez, FastJet user manual, *Eur. Phys. J. C* **72**, 1896 (2012).
- [78] ATLAS Collaboration, Topological cell clustering in the ATLAS calorimeters and its performance in LHC Run 1, *Eur. Phys. J. C* **77**, 490 (2017).
- [79] ATLAS Collaboration, Determination of jet calibration and energy resolution in proton–proton collisions at $\sqrt{s} = 8$ TeV using the ATLAS detector, *Eur. Phys. J. C* **80**, 1104 (2020).
- [80] ATLAS Collaboration, Jet energy scale measurements and their systematic uncertainties in proton–proton collisions at $\sqrt{s} = 13$ TeV with the ATLAS detector, *Phys. Rev. D* **96**, 072002 (2017).
- [81] ATLAS Collaboration, Selection of jets produced in 13 TeV proton–proton collisions with the ATLAS detector, Report No. ATLAS-CONF-2015-029, 2015, <https://cds.cern.ch/record/2037702>.
- [82] ATLAS Collaboration, Performance of pile-up mitigation techniques for jets in pp collisions at $\sqrt{s} = 8$ TeV using the ATLAS detector, *Eur. Phys. J. C* **76**, 581 (2016).
- [83] ATLAS Collaboration, Measurements of b -jet tagging efficiency with the ATLAS detector using $t\bar{t}$ events at $\sqrt{s} = 13$ TeV, *J. High Energy Phys.* **08** (2018) 089.
- [84] G. Aad *et al.* (ATLAS Collaboration), ATLAS b -jet identification performance and efficiency measurement with $t\bar{t}$ events in pp collisions at $\sqrt{s} = 13$ TeV, *Eur. Phys. J. C* **79**, 970 (2019).
- [85] ATLAS Collaboration, Performance of missing transverse momentum reconstruction with the ATLAS detector using proton–proton collisions at $\sqrt{s} = 13$ TeV, *Eur. Phys. J. C* **78**, 903 (2018).
- [86] ATLAS Collaboration, E_T^{miss} performance in the ATLAS detector using 2015–2016 LHC pp collisions, Report No. ATLAS-CONF-2018-023, 2018, <https://cds.cern.ch/record/2625233>.
- [87] ATLAS Collaboration, Search for a heavy charged boson in events with a charged lepton and missing transverse momentum from pp collisions at $\sqrt{s} = 13$ TeV with the ATLAS detector, *Phys. Rev. D* **100**, 052013 (2019).
- [88] ATLAS Collaboration, Tools for estimating fake/non-prompt lepton backgrounds with the ATLAS detector at the LHC, [arXiv:2211.16178](https://arxiv.org/abs/2211.16178).
- [89] M. Baak, G. J. Besjes, D. Côté, A. Koutsman, J. Lorenz, and D. Short, HistFitter software framework for statistical data analysis, *Eur. Phys. J. C* **75**, 153 (2015).
- [90] G. Cowan, K. Cranmer, E. Gross, and O. Vitells, Asymptotic formulae for likelihood-based tests of new physics, *Eur. Phys. J. C* **71**, 1554 (2011).
- [91] A. L. Read, Presentation of search results: The CL_S technique, *J. Phys. G* **28**, 2693 (2002).
- [92] ATLAS Collaboration, Measurement of the inelastic proton–proton cross section at $\sqrt{s} = 13$ TeV with the ATLAS detector at the LHC, *Phys. Rev. Lett.* **117**, 182002 (2016).
- [93] ATLAS Collaboration, ATLAS computing acknowledgements, Report No. ATL-SOFT-PUB-2023-001, 2023, <https://cds.cern.ch/record/2869272>.

G. Aad¹⁰³, B. Abbott¹²¹, D. C. Abbott¹⁰⁴, A. Abed Abud³⁶, K. Abeling⁵⁵, D. K. Abhayasinghe⁹⁵, S. H. Abidi¹⁵⁸, O. S. AbouZeid⁴², N. L. Abraham¹⁴⁸, H. Abramowicz¹⁵³, H. Abreu¹⁵², Y. Abulaiti⁶, B. S. Acharya^{69a,69b}, B. Achkar⁵⁵, L. Adam¹⁰¹, C. Adam Bourdarios⁵, L. Adamczyk^{85a}, L. Adamek¹⁵⁸, J. Adelman¹¹⁷, M. Adersberger¹¹⁰, A. Adiguzel^{12c,e}, S. Adorni⁵⁶, T. Adye¹³⁵, A. A. Affolder¹³⁷, Y. Afik¹⁵², C. Agapopoulou⁶⁷, M. N. Agaras⁴⁰, A. Aggarwal¹¹⁵, C. Agheorghiesei^{27c}, J. A. Aguilar-Saavedra^{131f,131a,d}, A. Ahmad³⁶, F. Ahmadov^{38,e}, W. S. Ahmed¹⁰⁵, X. Ai^{18a}, G. Aielli^{76a,76b}, S. Akatsuka⁸⁷, M. Akbiyik¹⁰¹, T. P. A. Åkesson⁹⁸, E. Akilli⁵⁶, A. V. Akimov³⁷, K. Al Houry⁶⁷, G. L. Alberghi^{23b}, J. Albert¹⁶⁷, M. J. Alconada Verzini¹⁵³, S. Alderweireldt³⁶, M. Aleksa³⁶, I. N. Aleksandrov³⁸, C. Alexa^{27b}, T. Alexopoulos¹⁰, A. Alfonsi¹¹⁶, F. Alfonsi^{23b,23a}, M. Alhroob¹²¹, B. Ali¹³³, S. Ali¹⁵⁰, M. Aliev³⁷, G. Alimonti^{71a}, C. Allaire³⁶, B. M. M. Allbrooke¹⁴⁸, B. W. Allen¹²⁴, P. P. Allport²¹, A. Aloisio^{72a,72b}, F. Alonso⁹⁰, C. Alpigiani¹⁴⁰, E. Alunno Camelia^{76a,76b}, M. Alvarez Estevez¹⁰⁰, M. G. Alvigi^{72a,72b}, Y. Amaral Coutinho^{82b}, A. Ambler¹⁰⁵, L. Ambroz¹²⁷, C. Amelung²⁶, D. Amidei¹⁰⁷, S. P. Amor Dos Santos^{131a}, S. Amoroso⁴⁸, C. S. Amrouche⁵⁶, F. An⁸¹, C. Anastopoulos¹⁴¹, N. Andari¹³⁶, T. Andeen¹¹, J. K. Anders²⁰, S. Y. Andrean^{47a,47b}, A. Andreazza^{71a,71b}, V. Andrei^{63a}, C. R. Anelli¹⁶⁷, S. Angelidakis⁹, A. Angerami⁴¹, A. V. Anisenkov³⁷, A. Annovi^{74a}, C. Antel⁵⁶, M. T. Anthony¹⁴¹, E. Antipov¹²², M. Antonelli⁵³, D. J. A. Antrim¹⁶², F. Anulli^{75a}, M. Aoki⁸³, J. A. Aparisi Pozo¹⁶⁵, M. A. Aparo¹⁴⁸, L. Aperio Bella⁴⁸, N. Aranzabal³⁶, V. Araujo Ferraz^{82a}, R. Araujo Pereira^{82b}, C. Arcangeletti⁵³, A. T. H. Arce⁵¹, F. A. Arduh⁹⁰, J-F. Arguin¹⁰⁹, S. Argyropoulos⁵⁴, J.-H. Arling⁴⁸, A. J. Armbruster³⁶, A. Armstrong¹⁶², O. Arnaez¹⁵⁸, H. Arnold¹¹⁶, Z. P. Arrubarrena Tame¹¹⁰, G. Artoni¹²⁷, H. Asada¹¹³, K. Asai¹¹⁹, S. Asai¹⁵⁵, T. Asawatavonvanich¹⁵⁷, N. A. Asbah⁶¹, E. M. Asimakopoulou¹⁶³, L. Asquith¹⁴⁸, J. Assahsah^{35d}, K. Assamagan²⁹, R. Astalos^{28a}, R. J. Atkin^{33a}, M. Atkinson¹⁶⁴, N. B. Atlay¹⁹, H. Atmani⁶⁷, K. Augsten¹³³, V. A. Austrup¹⁷³, G. Avolio³⁶, M. K. Ayoub^{15a}, G. Azuelos^{109,f}, H. Bachacou¹³⁶, K. Bachas¹⁵⁴, M. Backes¹²⁷, F. Backman^{47a,47b}, P. Bagnaia^{75a,75b}, H. Bahrasemani¹⁴⁴, A. J. Bailey¹⁶⁵, V. R. Bailey¹⁶⁴, J. T. Baines¹³⁵, C. Bakalis¹⁰, O. K. Baker¹⁷⁴, P. J. Bakker¹¹⁶, E. Bakos¹⁶, D. Bakshi Gupta⁸, S. Balaji¹⁴⁹, R. Balasubramanian¹¹⁶, E. M. Baldin³⁷, P. Balek¹⁷¹, F. Balli¹³⁶, W. K. Balunas¹²⁷, J. Balz¹⁰¹, E. Banas⁸⁶, M. Bandieramonte¹³⁰, A. Bandyopadhyay²⁴, Sw. Banerjee^{172,g}, L. Barak¹⁵³, W. M. Barbe⁴⁰, E. L. Barberio¹⁰⁶, D. Barberis^{57b,57a}, M. Barbero¹⁰³, G. Barbour⁹⁶, T. Barillari¹¹¹, M-S. Barisits³⁶, J. Barkeloo¹²⁴, T. Barklow¹⁴⁵, R. Barnea¹⁵², B. M. Barnett¹³⁵, R. M. Barnett^{18a}, Z. Barnovska-Blenessy^{62a}, A. Baroncelli^{62a}, G. Barone²⁹, A. J. Barr¹²⁷, L. Barranco Navarro^{47a,47b}, F. Barreiro¹⁰⁰, J. Barreiro Guimarães da Costa^{15a}, U. Barron¹⁵³, S. Barsov³⁷, F. Bartels^{63a}, R. Bartoldus¹⁴⁵, G. Bartolini¹⁰³, A. E. Barton⁹¹, P. Bartos^{28a}, A. Basalae⁴⁸, A. Basan¹⁰¹, A. Bassalat^{67,h}, M. J. Basso¹⁵⁸, R. L. Bates⁵⁹, S. Batlamous^{35e}, J. R. Batley³², B. Batool¹⁴³, M. Battaglia¹³⁷, M. Bause^{75a,75b}, F. Bauer^{136,a}, P. Bauer²⁴, H. S. Bawa³¹, A. Bayirli^{12c}, J. B. Beacham⁵¹, T. Beau¹²⁸, P. H. Beauchemin¹⁶¹, F. Becherer⁵⁴, P. Bechtle²⁴, H. C. Beck⁵⁵, H. P. Beck^{20,i}, K. Becker¹⁶⁹, C. Becot⁴⁸, A. Beddall^{12d}, A. J. Beddall^{12a}, V. A. Bednyakov³⁸, M. Bedognetti¹¹⁶, C. P. Bee¹⁴⁷, T. A. Beermann¹⁷³, M. Begalli^{82b}, M. Begel²⁹, A. Behera¹⁴⁷, J. K. Behr⁴⁸, F. Beisiegel²⁴, M. Belfkir⁵, A. S. Bell⁹⁶, G. Bella¹⁵³, L. Bellagamba^{23b}, A. Bellerive³⁴, P. Bellos⁹, K. Beloborodov³⁷, K. Belotskiy³⁷, N. L. Belyaev³⁷, D. Benckekroun^{35a}, N. Benekos¹⁰, Y. Benhammou¹⁵³, D. P. Benjamin⁶, M. Benoit²⁹, J. R. Bensinger²⁶, S. Bentvelsen¹¹⁶, L. Beresford¹²⁷, M. Beretta⁵³, D. Berge¹⁹, E. Bergeas Kuutmann¹⁶³, N. Berger⁵, B. Bergmann¹³³, L. J. Bergsten²⁶, J. Beringer^{18a}, S. Berlendis⁷, G. Bernardi¹²⁸, C. Bernius¹⁴⁵, F. U. Bernlochner²⁴, T. Berry⁹⁵, P. Berta¹⁰¹, A. Berthold⁵⁰, I. A. Bertram⁹¹, O. Bessidskaia Bylund¹⁷³, N. Besson¹³⁶, A. Bethani¹⁰², S. Bethke¹¹¹, A. Betti⁴⁴, A. J. Bevan⁹⁴, J. Beyer¹¹¹, D. S. Bhattacharya¹⁶⁸, P. Bhattarai²⁶, V. S. Bhopatkar⁶, R. Bi¹³⁰, R. M. Bianchi¹³⁰, O. Biebel¹¹⁰, D. Biedermann¹⁹, R. Bielski³⁶, K. Bierwagen¹⁰¹, N. V. Biesuz^{74a,74b}, M. Biglietti^{77a}, T. R. V. Billoud¹³³, M. Bindi⁵⁵, A. Bingul^{12d}, C. Bini^{75a,75b}, S. Biondi^{23b,23a}, C. J. Birch-sykes¹⁰², M. Birman¹⁷¹, T. Bisanz³⁶, D. Biswas^{172,g}, A. Bitadze¹⁰², C. Bittrich⁵⁰, K. Björke¹²⁶, T. Blazek^{28a}, I. Bloch⁴⁸, C. Blocker²⁶, A. Blue⁵⁹, U. Blumenschein⁹⁴, J. Blumenthal¹⁰¹, G. J. Bobbink¹¹⁶, V. S. Bobrovnikov³⁷, S. S. Bocchetta⁹⁸, D. Bogavac¹⁴, A. G. Bogdanchikov³⁷, C. Bohm^{47a}, V. Boisvert⁹⁵, P. Boka^{163,55}, T. Bold^{85a}, A. E. Bolz^{63b}, M. Bomben¹²⁸, M. Bona⁹⁴, J. S. Bonilla¹²⁴, M. Boonekamp¹³⁶, C. D. Booth⁹⁵, A. G. Borbély⁵⁹, H. M. Borecka-Bielska⁹², L. S. Borgna⁹⁶, A. Borisov³⁷, G. Borissov⁹¹, D. Bortoletto¹²⁷, D. Boscherini^{23b}, M. Bosman¹⁴, J. D. Bossio Sola¹⁰⁵, K. Bouaouda^{35a}, J. Boudreau¹³⁰, E. V. Bouhova-Thacker⁹¹, D. Boumediene⁴⁰, A. Boveia¹²⁰, J. Boyd³⁶, D. Boye^{33c}

I. R. Boyko³⁸ A. J. Bozson⁹⁵ J. Bracinek²¹ N. Brahimi^{62d,62c} G. Brandt¹⁷³ O. Brandt³² F. Braren⁴⁸
 B. Brau¹⁰⁴ J. E. Brau¹²⁴ W. D. Breaden Madden⁵⁹ K. Brendlinger⁴⁸ R. Brener¹⁵² L. Brenner³⁶ R. Brenner¹⁶³
 S. Bressler¹⁷¹ B. Brickwedde¹⁰¹ D. L. Briglin²¹ D. Britton⁵⁹ D. Britzger¹¹¹ I. Brock²⁴ R. Brock¹⁰⁸
 G. Brooijmans⁴¹ W. K. Brooks^{138d} E. Brost²⁹ P. A. Bruckman de Renstrom⁸⁶ B. Brüers⁴⁸ D. Bruncko^{28b,a}
 A. Bruni^{23b} G. Bruni^{23b} M. Bruschi^{23b} N. Bruscolo^{75a,75b} L. Bryngemark¹⁴⁵ T. Buanes¹⁷ Q. Buat¹⁴⁷
 P. Buchholz¹⁴³ A. G. Buckley⁵⁹ I. A. Budagov^{38,a} M. K. Bugge¹²⁶ F. Bühner⁵⁴ O. Bulekov³⁷ B. A. Bullard⁶¹
 T. J. Burch¹¹⁷ S. Burdin⁹² C. D. Burgard¹¹⁶ A. M. Burger¹²² B. Burghgrave⁸ J. T. P. Burr⁴⁸ C. D. Burton¹¹
 J. C. Burzynski¹⁰⁴ V. Büscher¹⁰¹ E. Buschmann⁵⁵ P. J. Bussey⁵⁹ J. M. Butler²⁵ C. M. Buttar⁵⁹
 J. M. Butterworth⁹⁶ P. Butti³⁶ W. Buttinger³⁶ C. J. Buxo Vazquez¹⁰⁸ A. Buzatu¹⁵⁰ A. R. Buzykaev³⁷
 G. Cabras^{23b,23a} S. Cabrera Urbán¹⁶⁵ D. Caforio⁵⁸ H. Cai¹³⁰ V. M. M. Cairo¹⁴⁵ O. Cakir^{4a} N. Calace³⁶
 P. Calafiura^{18a} G. Calderini¹²⁸ P. Calfayan⁶⁸ G. Callea⁵⁹ L. P. Caloba^{82b} A. Caltabiano^{76a,76b}
 S. Calvente Lopez¹⁰⁰ D. Calvet⁴⁰ S. Calvet⁴⁰ T. P. Calvet¹⁰³ M. Calvetti^{74a,74b} R. Camacho Toro¹²⁸
 S. Camarda³⁶ D. Camarero Munoz¹⁰⁰ P. Camarri^{76a,76b} M. T. Camerlingo^{77a,77b} D. Cameron¹²⁶
 C. Camincher³⁶ S. Campana³⁶ M. Campanelli⁹⁶ A. Camplani⁴² V. Canale^{72a,72b} A. Canesse¹⁰⁵
 M. Cano Bret⁸⁰ J. Cantero¹²² T. Cao¹⁵³ Y. Cao¹⁶⁴ M. D. M. Capeans Garrido³⁶ M. Capua^{43b,43a}
 R. Cardarelli^{76a} F. Cardillo¹⁴¹ I. Carli¹³⁴ T. Carli³⁶ G. Carlino^{72a} B. T. Carlson¹³⁰ E. M. Carlson^{167,159a}
 L. Carminati^{71a,71b} R. M. D. Carney¹⁴⁵ S. Caron¹¹⁵ E. Carquin^{138d} S. Carrá⁴⁸ G. Carratta^{23b,23a}
 J. W. S. Carter¹⁵⁸ T. M. Carter⁵² M. P. Casado^{14,j} A. F. Casha¹⁵⁸ E. G. Castiglia¹⁷⁴ F. L. Castillo¹⁶⁵
 L. Castillo Garcia¹⁴ V. Castillo Gimenez¹⁶⁵ N. F. Castro^{131a,131e} A. Catinaccio³⁶ J. R. Catmore¹²⁶ A. Cattai³⁶
 V. Cavaliere²⁹ V. Cavasinni^{74a,74b} E. Celebi^{12b} F. Celli¹²⁷ K. Cerny¹²³ A. S. Cerqueira^{82a} A. Cerri¹⁴⁸
 L. Cerrito^{76a,76b} F. Cerutti^{18a} A. Cervelli^{23b} S. A. Cetin^{12b} Z. Chadi^{35a} D. Chakraborty¹¹⁷ J. Chan¹⁷²
 W. S. Chan¹¹⁶ W. Y. Chan⁹² J. D. Chapman³² B. Chargeishvili^{151b} D. G. Charlton²¹ T. P. Charman⁹⁴
 M. Chatterjee²⁰ C. C. Chau³⁴ S. Che¹²⁰ S. Chekanov⁶ S. V. Chekulaev^{159a} G. A. Chelkov^{38,k} B. Chen⁸¹
 C. Chen^{62a} C. H. Chen⁸¹ H. Chen^{15c} H. Chen²⁹ J. Chen^{62a} J. Chen⁴¹ J. Chen²⁶ S. Chen¹²⁹ S. J. Chen^{15c}
 X. Chen^{15b,l} Y. Chen^{62a} Y-H. Chen⁴⁸ H. C. Cheng^{65a} H. J. Cheng^{15a} A. Cheplakov³⁸ E. Cheremushkina³⁷
 R. Cherkaoui El Moursli^{35e} E. Cheu⁷ K. Cheung⁶⁶ T. J. A. Chevalérias¹³⁶ L. Chevalier¹³⁶ V. Chiarella⁵³
 G. Chiarelli^{74a} G. Chiodini^{70a} A. S. Chisholm²¹ A. Chitan^{27b} I. Chiu¹⁵⁵ Y. H. Chiu¹⁶⁷ M. V. Chizhov³⁸
 K. Choi¹¹ A. R. Chomont^{75a,75b} E. Y. S. Chow¹¹⁶ L. D. Christopher^{33e} M. C. Chu^{65a} X. Chu^{15a,15d}
 J. Chudoba¹³² J. J. Chwastowski⁸⁶ L. Chytka¹²³ D. Cieri¹¹¹ K. M. Ciesla⁸⁶ V. Cindro⁹³ I. A. Cioară^{27b}
 A. Ciocio^{18a} F. Ciroto^{72a,72b} Z. H. Citron^{171,m} M. Citterio^{71a} D. A. Ciubotaru^{27b} B. M. Ciungu¹⁵⁸ A. Clark⁵⁶
 M. R. Clark⁴¹ P. J. Clark⁵² S. E. Clawson¹⁰² C. Clement^{47a,47b} Y. Coadou¹⁰³ M. Cobal^{69a,69c} A. Coccaro^{57b}
 J. Cochran⁸¹ R. Coelho Lopes De Sa¹⁰⁴ H. Cohen¹⁵³ A. E. C. Coimbra³⁶ B. Cole⁴¹ A. P. Colijn¹¹⁶ J. Collot⁶⁰
 P. Conde Muiño^{131a,131h} S. H. Connell^{33c} I. A. Connelly⁵⁹ S. Constantinescu^{27b} F. Conventi^{72a,n}
 A. M. Cooper-Sarkar¹²⁷ F. Cormier¹⁶⁶ K. J. R. Cormier¹⁵⁸ L. D. Corpe⁹⁶ M. Corradi^{75a,75b} E. E. Corrigan⁹⁸
 F. Corriveau^{105,o} M. J. Costa¹⁶⁵ F. Costanza⁵ D. Costanzo¹⁴¹ G. Cowan⁹⁵ J. W. Cowley³² J. Crane¹⁰²
 K. Cranmer¹¹⁸ R. A. Creager¹²⁹ S. Crépe-Renaudin⁶⁰ F. Crescioli¹²⁸ M. Cristinziani²⁴ V. Croft¹⁶¹
 G. Crosetti^{43b,43a} A. Cueto⁵ T. Cuhadar Donszelmann¹⁶² H. Cui^{15a,15d} A. R. Cukierman¹⁴⁵
 W. R. Cunningham⁵⁹ S. Czekierda⁸⁶ P. Czodrowski³⁶ M. M. Czurylo^{63b} M. J. Da Cunha Sargedas De Sousa^{62b}
 J. V. Da Fonseca Pinto^{82b} C. Da Via¹⁰² W. Dabrowski^{85a} F. Dachs³⁶ T. Dado⁴⁹ S. Dahbi^{33e} T. Dai¹⁰⁷
 C. Dallapiccola¹⁰⁴ M. Dam⁴² G. D'amen²⁹ V. D'Amico^{77a,77b} J. Damp¹⁰¹ J. R. Dandoy¹²⁹ M. F. Daneri³⁰
 M. Danninger¹⁴⁴ V. Dao³⁶ G. Darbo^{57b} O. Dartsis⁵ A. Dattagupta¹²⁴ T. Daubney⁴⁸ S. D'Auria^{71a,71b}
 C. David^{159b} T. Davidek¹³⁴ D. R. Davis⁵¹ I. Dawson¹⁴¹ K. De⁸ R. De Asmundis^{72a} M. De Beurs¹¹⁶
 S. De Castro^{23b,23a} N. De Groot¹¹⁵ P. de Jong¹¹⁶ H. De la Torre¹⁰⁸ A. De Maria^{15c} D. De Pedis^{75a}
 A. De Salvo^{75a} U. De Sanctis^{76a,76b} M. De Santis^{76a,76b} A. De Santo¹⁴⁸ J. B. De Vivie De Regie⁶⁷
 D. V. Dedovich³⁸ A. M. Deiana⁴⁴ J. Del Peso¹⁰⁰ Y. Delabat Diaz⁴⁸ D. Delgove⁶⁷ F. Deliot¹³⁶ C. M. Delitzsch⁷
 M. Della Pietra^{72a,72b} D. Della Volpe⁵⁶ A. Dell'Acqua³⁶ L. Dell'Asta^{76a,76b} M. Delmastro⁵ C. Delporte⁶⁷
 P. A. Delsart⁶⁰ D. A. DeMarco¹⁵⁸ S. Demers¹⁷⁴ M. Demichev³⁸ G. Demontigny¹⁰⁹ S. P. Denisov³⁷
 L. D'Eramo¹¹⁷ D. Derendarz⁸⁶ J. E. Derkaoui^{35d} F. Derue¹²⁸ P. Dervan⁹² K. Desch²⁴ K. Dette¹⁵⁸
 C. Deutsch²⁴ M. R. Devesa³⁰ P. O. Deviveiros³⁶ F. A. Di Bello^{75a,75b} A. Di Ciaccio^{76a,76b} L. Di Ciaccio⁵

W. K. Di Clemente¹²⁹ C. Di Donato^{72a,72b} A. Di Girolamo³⁶ G. Di Gregorio^{74a,74b} B. Di Micco^{77a,77b}
 R. Di Nardo^{77a,77b} R. Di Sipio¹⁵⁸ C. Diaconu¹⁰³ F. A. Dias¹¹⁶ T. Dias Do Vale^{131a} M. A. Diaz^{138a}
 F. G. Diaz Capriles²⁴ J. Dickinson^{18a} M. Didenko³⁷ E. B. Diehl¹⁰⁷ J. Dietrich¹⁹ S. Díez Cornell⁴⁸
 C. Diez Pardos¹⁴³ A. Dimitrievska^{18a} W. Ding^{15b} J. Dingfelder²⁴ S. J. Dittmeier^{63b} F. Dittus³⁶ F. Djama¹⁰³
 T. Djobava^{151b} J. I. Djuvsland¹⁷ M. A. B. Do Vale¹³⁹ M. Dobre^{27b} D. Dodsworth²⁶ C. Doglioni⁹⁸
 J. Dolejsi¹³⁴ Z. Dolezal¹³⁴ M. Donadelli^{82c} B. Dong^{62c} J. Donini⁴⁰ A. D'Onofrio^{15c} M. D'Onofrio⁹²
 J. Dopke¹³⁵ A. Doria^{72a} M. T. Dova⁹⁰ A. T. Doyle⁵⁹ E. Drechsler¹⁴⁴ E. Dreyer¹⁴⁴ T. Dreyer⁵⁵
 A. S. Drobac¹⁶¹ D. Du^{62b} T. A. du Pree¹¹⁶ Y. Duan^{62d} F. Dubinin³⁷ M. Dubovsky^{28a} A. Dubreuil⁵⁶
 E. Duchovni¹⁷¹ G. Duckeck¹¹⁰ O. A. Ducu^{36,27b} D. Duda¹¹¹ A. Dudarev³⁶ A. C. Dudder¹⁰¹ E. M. Duffield^{18a}
 M. D'uffizi¹⁰² L. Duflot⁶⁷ M. Dührssen³⁶ C. Dülsen¹⁷³ M. Dumancic¹⁷¹ A. E. Dumitriu^{27b} M. Dunford^{63a}
 A. Duperrin¹⁰³ H. Duran Yildiz^{4a} M. Düren⁵⁸ A. Durglishvili^{151b} D. Duschinger⁵⁰ B. Dutta⁴⁸ B. L. Dwyer¹¹⁷
 G. I. Dyckes¹²⁹ M. Dyndal³⁶ S. Dysch¹⁰² B. S. Dziedzic⁸⁶ M. G. Eggleston⁵¹ T. Eifert⁸ G. Eigen¹⁷
 K. Einsweiler^{18a} T. Ekelof¹⁶³ H. El Jarrari^{35e} V. Ellajosyula¹⁶³ M. Ellert¹⁶³ F. Ellinghaus¹⁷³ A. A. Elliot⁹⁴
 N. Ellis³⁶ J. Elmsheuser²⁹ M. Elsing³⁶ D. Emelianov¹³⁵ A. Emerman⁴¹ Y. Enari¹⁵⁵ M. B. Epland⁵¹
 J. Erdmann⁴⁹ A. Ereditato²⁰ P. A. Erland⁸⁶ M. Errenst¹⁷³ M. Escalier⁶⁷ C. Escobar¹⁶⁵ O. Estrada Pastor¹⁶⁵
 E. Etzion¹⁵³ H. Evans⁶⁸ M. O. Evans¹⁴⁸ A. Ezhilov³⁷ F. Fabbri⁵⁹ L. Fabbri^{23b,23a} V. Fabiani¹¹⁵
 G. Facini¹⁶⁹ R. M. Fakhruddinov³⁷ S. Falciano^{75a} P. J. Falke²⁴ S. Falke³⁶ J. Faltova¹³⁴ Y. Fang^{15a}
 Y. Fang^{15a,15d} G. Fanourakis⁴⁶ M. Fanti^{71a,71b} M. Faraj^{69a,69c} A. Farbin⁸ A. Farilla^{77a} E. M. Farina^{73a,73b}
 T. Faroouque¹⁰⁸ S. M. Farrington⁵² P. Farthouat³⁶ F. Fassi^{35e} P. Fassnacht³⁶ D. Fassouliotis⁹
 M. Fauci Giannelli⁵² W. J. Fawcett³² L. Fayard⁶⁷ O. L. Fedin^{37,k} W. Fedorko¹⁶⁶ M. Feickert¹⁶⁴
 L. Felgioni¹⁰³ A. Fell¹⁴¹ C. Feng^{62b} M. Feng⁵¹ M. J. Fenton¹⁶² A. B. Fenyuk³⁷ S. W. Ferguson⁴⁵
 J. Ferrando⁴⁸ A. Ferrante¹⁶⁴ A. Ferrari¹⁶³ P. Ferrari¹¹⁶ R. Ferrari^{73a} D. E. Ferreira de Lima^{63b} A. Ferrer¹⁶⁵
 D. Ferrere⁵⁶ C. Ferretti¹⁰⁷ F. Fiedler¹⁰¹ A. Filipčić⁹³ F. Filthaut¹¹⁵ K. D. Finelli²⁵ M. C. N. Fiolhais^{131a,131c,p}
 L. Fiorini¹⁶⁵ F. Fischer¹¹⁰ W. C. Fisher¹⁰⁸ T. Fitschen²¹ I. Fleck¹⁴³ P. Fleischmann¹⁰⁷ T. Flick¹⁷³
 B. M. Flierl¹¹⁰ L. Flores¹²⁹ L. R. Flores Castillo^{65a} F. M. Follega^{78a,78b} N. Fomin¹⁷ J. H. Foo¹⁵⁸
 G. T. Forcolin^{78a,78b} B. C. Forland⁶⁸ A. Formica¹³⁶ F. A. Förster¹⁴ A. C. Forti¹⁰² E. Fortin¹⁰³ M. G. Foti¹²⁷
 D. Fournier⁶⁷ H. Fox⁹¹ P. Francavilla^{74a,74b} S. Francescato^{75a,75b} M. Franchini^{23b,23a} S. Franchino^{63a}
 D. Francis³⁶ L. Franco⁵ L. Franconi²⁰ M. Franklin⁶¹ G. Frattari^{75a,75b} A. N. Fray⁹⁴ P. M. Freeman²¹
 B. Freund¹⁰⁹ W. S. Freund^{82b} E. M. Freundlich⁴⁹ D. C. Frizzell¹²¹ D. Froidevaux³⁶ J. A. Frost¹²⁷
 M. Fujimoto¹¹⁹ C. Fukunaga¹⁵⁶ E. Fullana Torregrosa^{165,a} T. Fusayasu¹¹² J. Fuster¹⁶⁵ A. Gabrielli^{23b,23a}
 A. Gabrielli³⁶ S. Gadatsch⁵⁶ P. Gadow¹¹¹ G. Gagliardi^{57b,57a} L. G. Gagnon¹⁰⁹ G. E. Gallardo¹²⁷
 E. J. Gallas¹²⁷ B. J. Gallop¹³⁵ R. Gamboa Goni⁹⁴ K. K. Gan¹²⁰ S. Ganguly¹⁷¹ J. Gao^{62a} Y. Gao⁵²
 Y. S. Gao^{31,q} F. M. Garay Walls^{138a} C. García¹⁶⁵ J. E. García Navarro¹⁶⁵ J. A. García Pascual^{15a}
 C. Garcia-Argos⁵⁴ M. Garcia-Sciveres^{18a} R. W. Gardner³⁹ S. Gargiulo⁵⁴ C. A. Garner¹⁵⁸ V. Garonne¹²⁶
 S. J. Gasiorowski¹⁴⁰ P. Gaspar^{82b} A. Gaudiello^{57b,57a} G. Gaudio^{73a} P. Gauzzi^{75a,75b} I. L. Gavrilenko³⁷
 A. Gavriluk³⁷ C. Gay¹⁶⁶ G. Gaycken⁴⁸ E. N. Gazis¹⁰ A. A. Geanta^{27b} C. M. Gee¹³⁷ C. N. P. Gee¹³⁵
 J. Geisen⁹⁸ M. Geisen¹⁰¹ C. Gemme^{57b} M. H. Genest⁶⁰ C. Geng¹⁰⁷ S. Gentile^{75a,75b} S. George⁹⁵ T. Gerialis⁴⁶
 L. O. Gerlach⁵⁵ P. Gessinger-Befurt¹⁰¹ G. Gessner⁴⁹ S. Ghasemi¹⁴³ M. Ghasemi Bostanabad¹⁶⁷ M. Ghneimat¹⁴³
 A. Ghosh⁶⁷ A. Ghosh⁸⁰ B. Giacobbe^{23b} S. Giagu^{75a,75b} N. Giangiacomi^{23b,23a} P. Giannetti^{74a}
 A. Giannini^{72a,72b} G. Giannini¹⁴ S. M. Gibson⁹⁵ M. Gignac¹³⁷ D. T. Gil^{85b} B. J. Gilbert⁴¹ D. Gillberg³⁴
 G. Gilles¹⁷³ D. M. Gingrich^{3,f} M. P. Giordani^{69a,69c} P. F. Giraud¹³⁶ G. Giugliarelli^{69a,69c} D. Giugni^{71a}
 F. Giuli^{76a,76b} S. Gkaitatzis¹⁵⁴ I. Gkialas^{9,r} E. L. Gkoukousis¹⁴ P. Gkoutoumis¹⁰ L. K. Gladilin³⁷
 C. Glasman¹⁰⁰ J. Glatzer¹⁴ P. C. F. Glaysher⁴⁸ A. Glazov⁴⁸ G. R. Gledhill¹²⁴ I. Gnesi^{43b,s} M. Goblirsch-Kolb²⁶
 D. Godin¹⁰⁹ S. Goldfarb¹⁰⁶ T. Golling⁵⁶ D. Golubkov³⁷ A. Gomes^{131a,131b} R. Goncalves Gama⁵⁵
 R. Gonçalves^{131a,131c} G. Gonella¹²⁴ L. Gonella²¹ A. Gongadze³⁸ F. Gonnella²¹ J. L. Gonski⁴¹
 S. González de la Hoz¹⁶⁵ S. Gonzalez Fernandez¹⁴ R. Gonzalez Lopez⁹² C. Gonzalez Renteria^{18a}
 R. Gonzalez Suarez¹⁶³ S. Gonzalez-Sevilla⁵⁶ G. R. Gonzalvo Rodriguez¹⁶⁵ L. Goossens³⁶ N. A. Gorasia²¹
 P. A. Gorbounov³⁷ B. Gorini³⁶ E. Gorini^{70a,70b} A. Gorišek⁹³ A. T. Goshaw⁵¹ M. I. Gostkin³⁸
 C. A. Gottardo¹¹⁵ M. Goughri^{35b} A. G. Goussiou¹⁴⁰ N. Govender^{33c} C. Goy⁵ I. Grabowska-Bold^{85a}

E. C. Graham⁹², J. Gramling¹⁶², E. Gramstad¹²⁶, S. Grancagnolo¹⁹, M. Grandi¹⁴⁸, V. Gratchev^{37,a}, P. M. Gravila^{27f},
 F. G. Gravili^{70a,70b}, C. Gray⁵⁹, H. M. Gray^{18a}, C. Grefe²⁴, K. Gregersen⁹⁸, I. M. Gregor⁴⁸, P. Grenier¹⁴⁵,
 K. Grevtsov⁴⁸, C. Grieco¹⁴, N. A. Grieser¹²¹, A. A. Grillo¹³⁷, K. Grimm^{31,t}, S. Grinstein^{14,u}, J.-F. Grivaz⁶⁷,
 S. Groh¹⁰¹, E. Gross¹⁷¹, J. Grosse-Knetter⁵⁵, Z. J. Grout⁹⁶, C. Grud¹⁰⁷, A. Grummer¹¹⁴, J. C. Grundy¹²⁷,
 L. Guan¹⁰⁷, W. Guan¹⁷², C. Gubbels¹⁶⁶, J. Guenther³⁶, A. Guerguichon⁶⁷, J. G. R. Guerrero Rojas¹⁶⁵,
 F. Guescini¹¹¹, R. Gugel¹⁰¹, A. Guida⁴⁸, T. Guillemin⁵, S. Guindon³⁶, J. Guo^{62c}, W. Guo¹⁰⁷, Y. Guo^{62a},
 Z. Guo¹⁰³, R. Gupta⁴⁸, S. Gurbuz^{12c}, G. Gustavino¹²¹, M. Guth⁵⁴, P. Gutierrez¹²¹, C. Gutsche⁹⁶, C. Guyot¹³⁶,
 C. Gwenlan¹²⁷, C. B. Gwilliam⁹², E. S. Haaland¹²⁶, A. Haas¹¹⁸, C. Haber^{18a}, H. K. Hadavand⁸, A. Hadeef^{62a},
 M. Haleem¹⁶⁸, J. Haley¹²², J. J. Hall¹⁴¹, G. Halladjian¹⁰⁸, G. D. Hallewell¹⁰³, K. Hamano¹⁶⁷, H. Hamdaoui^{35e},
 M. Hamer²⁴, G. N. Hamity⁵², K. Han^{62a,v}, L. Han^{15c}, L. Han^{62a}, S. Han^{18a}, Y. F. Han¹⁵⁸, K. Hanagaki⁸³,
 M. Hance¹³⁷, D. M. Handl¹¹⁰, M. D. Hank³⁹, R. Hankache¹²⁸, E. Hansen⁹⁸, J. B. Hansen⁴², J. D. Hansen⁴²,
 M. C. Hansen²⁴, P. H. Hansen⁴², E. C. Hanson¹⁰², K. Hara¹⁶⁰, T. Harenberg¹⁷³, S. Harkusha³⁷, P. F. Harrison¹⁶⁹,
 N. M. Hartman¹⁴⁵, N. M. Hartmann¹¹⁰, Y. Hasegawa¹⁴², A. Hasib⁵², S. Hassani¹³⁶, S. Haug²⁰, R. Hauser¹⁰⁸,
 L. B. Havener⁴¹, M. Havranek¹³³, C. M. Hawkes²¹, R. J. Hawkings³⁶, S. Hayashida¹¹³, D. Hayden¹⁰⁸,
 C. Hayes¹⁰⁷, R. L. Hayes¹⁶⁶, C. P. Hays¹²⁷, J. M. Hays⁹⁴, H. S. Hayward⁹², S. J. Haywood¹³⁵, F. He^{62a},
 Y. He¹⁵⁷, M. P. Heath⁵², V. Hedberg⁹⁸, S. Heer²⁴, A. L. Heggelund¹²⁶, C. Heidegger⁵⁴, K. K. Heidegger⁵⁴,
 W. D. Heidorn⁸¹, J. Heilman³⁴, S. Heim⁴⁸, T. Heim^{18a}, B. Heinemann^{48,w}, J. G. Heinlein¹²⁹, J. J. Heinrich¹²⁴,
 L. Heinrich³⁶, J. Hejbal¹³², L. Helary⁴⁸, A. Held¹¹⁸, S. Hellesund¹²⁶, C. M. Helling¹³⁷, S. Hellman^{47a,47b},
 C. Helsen³⁶, R. C. W. Henderson⁹¹, Y. Heng¹⁷², L. Henkelmann³², A. M. Henriques Correia³⁶, H. Herde²⁶,
 Y. Hernández Jiménez^{33e}, H. Herr¹⁰¹, M. G. Herrmann¹¹⁰, T. Herrmann⁵⁰, G. Herten⁵⁴, R. Hertenberger¹¹⁰,
 L. Hervas³⁶, T. C. Herwig¹²⁹, G. G. Hesketh⁹⁶, N. P. Hessey^{159a}, H. Hibi⁸⁴, S. Higashino⁸³,
 E. Higón-Rodríguez¹⁶⁵, K. Hildebrand³⁹, J. C. Hill³², K. K. Hill²⁹, K. H. Hiller⁴⁸, S. J. Hillier²¹, M. Hils⁵⁰,
 I. Hinchliffe^{18a}, F. Hinterkeuser²⁴, M. Hirose¹²⁵, S. Hirose¹⁶⁰, D. Hirschbuehl¹⁷³, B. Hiti⁹³, O. Hladik¹³²,
 J. Hobbs¹⁴⁷, N. Hod¹⁷¹, M. C. Hodgkinson¹⁴¹, A. Hoecker³⁶, D. Hohn⁵⁴, D. Hohov⁶⁷, T. Holm²⁴,
 T. R. Holmes³⁹, M. Holzbock¹¹¹, L. B. A. H. Hommels³², T. M. Hong¹³⁰, J. C. Honig⁵⁴, A. Hönle¹¹¹,
 B. H. Hooberman¹⁶⁴, W. H. Hopkins⁶, Y. Horii¹¹³, P. Horn⁵⁰, L. A. Horyn³⁹, S. Hou¹⁵⁰, A. Hoummada^{35a},
 J. Howarth⁵⁹, J. Hoya⁹⁰, M. Hrabovsky¹²³, J. Hrdinka⁷⁹, J. Hrivnac⁶⁷, A. Hrynevich³⁷, T. Hryn'ova⁵, P. J. Hsu⁶⁶,
 S.-C. Hsu¹⁴⁰, Q. Hu²⁹, S. Hu^{62c}, Y. F. Hu^{15a,15d,x}, D. P. Huang⁹⁶, X. Huang^{15c}, Y. Huang^{62a}, Y. Huang^{15a},
 Z. Hubacek¹³³, F. Hubaut¹⁰³, M. Huebner²⁴, F. Huettinger²⁴, T. B. Huffman¹²⁷, M. Huhtinen³⁶, R. Hulsken⁶⁰,
 R. F. H. Hunter³⁴, P. Huo¹⁴⁷, N. Huseynov^{38,e}, J. Huston¹⁰⁸, J. Huth⁶¹, R. Hyneman¹⁴⁵, S. Hyrych^{28a},
 G. Iacobucci⁵⁶, G. Iakovidis²⁹, I. Ibragimov¹⁴³, L. Iconomidou-Fayard⁶⁷, P. Iengo³⁶, R. Ignazzi⁴²,
 O. Igonkina^{116,a,y}, R. Iguchi¹⁵⁵, T. Iizawa⁵⁶, Y. Ikegami⁸³, M. Ikeno⁸³, A. Ilg²⁰, N. Ilic^{115,158,o}, F. Iltzsche⁵⁰,
 H. Imam^{35a}, G. Introzzi^{73a,73b}, M. Iodice^{77a}, K. Iordanidou^{159a}, V. Ippolito^{75a,75b}, M. F. Isacson¹⁶³, M. Ishino¹⁵⁵,
 W. Islam¹²², C. Issever^{19,48}, S. Istin¹⁵², J. M. Iturbe Ponce^{65a}, R. Iuppa^{78a,78b}, A. Ivina¹⁷¹, J. M. Izen⁴⁵,
 V. Izzo^{72a}, P. Jacka¹³², P. Jackson¹, R. M. Jacobs⁴⁸, B. P. Jaeger¹⁴⁴, V. Jain², G. Jäkel¹⁷³, K. B. Jakobi¹⁰¹,
 K. Jakobs⁵⁴, T. Jakoubek¹⁷¹, J. Jamieson⁵⁹, K. W. Janas^{85a}, R. Jansky⁵⁶, M. Janus⁵⁵, P. A. Janus^{85a},
 G. Jarlskog⁹⁸, A. E. Jaspan⁹², N. Javadov^{38,e}, T. Javůrek³⁶, M. Javurkova¹⁰⁴, F. Jeanneau¹³⁶, L. Jeanty¹²⁴,
 J. Jejelava^{151a,z}, P. Jenni^{54,aa}, N. Jeong⁴⁸, S. Jézéquel⁵, H. Ji¹⁷², J. Jia¹⁴⁷, Z. Jia^{15c}, H. Jiang⁸¹, Y. Jiang^{62a}, Z. Jiang¹⁴⁵,
 S. Jiggins⁵⁴, F. A. Jimenez Morales⁴⁰, J. Jimenez Pena¹¹¹, S. Jin^{15c}, A. Jinaru^{27b}, O. Jinnouchi¹⁵⁷, H. Jivan^{33e},
 P. Johansson¹⁴¹, K. A. Johns⁷, C. A. Johnson⁶⁸, E. Jones¹⁶⁹, R. W. L. Jones⁹¹, S. D. Jones¹⁴⁸, T. J. Jones⁹²,
 J. Jongmanns^{63a}, J. Jovicevic³⁶, X. Ju^{18a}, J. J. Junggeburth¹¹¹, A. Juste Rozas^{14,u}, A. Kaczmarzka⁸⁶,
 M. Kado^{75a,75b}, H. Kagan¹²⁰, M. Kagan¹⁴⁵, A. Kahn⁴¹, C. Kahra¹⁰¹, T. Kajji¹⁷⁰, E. Kajomovitz¹⁵²,
 C. W. Kalderon²⁹, A. Kaluza¹⁰¹, A. Kamenshchikov³⁷, M. Kaneda¹⁵⁵, N. J. Kang¹³⁷, S. Kang⁸¹, Y. Kano¹¹³,
 J. Kanzaki⁸³, L. S. Kaplan¹⁷², D. Kar^{33c}, K. Karava¹²⁷, M. J. Kareem^{159b}, I. Karkanas¹⁵⁴, S. N. Karpov³⁸,
 Z. M. Karpova³⁸, V. Kartvelishvili⁹¹, A. N. Karyukhin³⁷, E. Kasimi¹⁵⁴, A. Kastanas^{47a,47b}, C. Kato^{62d},
 J. Katzy⁴⁸, K. Kawade¹⁴², K. Kawagoe⁸⁹, T. Kawaguchi¹¹³, T. Kawamoto¹³⁶, G. Kawamura⁵⁵, E. F. Kay¹⁶⁷,
 S. Kazakos¹⁴, V. F. Kazanin³⁷, J. M. Keaveney^{33a}, R. Keeler¹⁶⁷, J. S. Keller³⁴, E. Kellermann⁹⁸, D. Kelsey¹⁴⁸,
 J. J. Kempster²¹, J. Kendrick²¹, K. E. Kennedy⁴¹, O. Kepka¹³², S. Kersten¹⁷³, B. P. Kerševan⁹³,
 S. Ketabchi Haghighat¹⁵⁸, M. Khader¹⁶⁴, F. Khalil-Zada¹³, M. Khandoga¹³⁶, A. Khanov¹²², A. G. Kharlamov³⁷

T. Kharlamova³⁷ E. E. Khoda¹⁶⁶ A. Khodinov³⁷ T. J. Khoo⁵⁶ G. Khorauli¹⁶⁸ J. Khubua^{151b} S. Kido⁸⁴
M. Kiehn³⁶ E. Kim¹⁵⁷ Y. K. Kim³⁹ N. Kimura⁹⁶ A. Kirchhoff⁵⁵ D. Kirchmeier⁵⁰ J. Kirk¹³⁵
A. E. Kiryunin¹¹¹ T. Kishimoto¹⁵⁵ D. P. Kisliuk¹⁵⁸ V. Kitali⁴⁸ C. Kitsaki¹⁰ O. Kivernyk²⁴
T. Klapdor-Kleingrothaus⁵⁴ M. Klassen^{63a} C. Klein³⁴ M. H. Klein¹⁰⁷ M. Klein⁹² U. Klein⁹²
K. Kleinknecht¹⁰¹ P. Klimek¹¹⁷ A. Klimentov²⁹ T. Klingl²⁴ T. Klioutchnikova³⁶ F. F. Klitzner¹¹⁰ P. Kluit¹¹⁶
S. Kluth¹¹¹ E. Kneringer⁷⁹ E. B. F. G. Knoops¹⁰³ A. Knue⁵⁴ D. Kobayashi⁸⁹ M. Kobel⁵⁰ M. Kocian¹⁴⁵
T. Kodama¹⁵⁵ P. Kodyš¹³⁴ D. M. Koeck¹⁴⁸ P. T. Koenig²⁴ T. Koffas³⁴ N. M. Köhler³⁶ M. Kolb¹³⁶
I. Koletsou⁵ T. Komarek¹²³ T. Kondo⁸³ K. Köneke⁵⁴ A. X. Y. Kong¹ A. C. König¹¹⁵ T. Kono¹¹⁹
V. Konstantinides⁹⁶ N. Konstantinidis⁹⁶ B. Konya⁹⁸ R. Kopeliansky⁶⁸ S. Koperny^{85a} K. Korcyl⁸⁶
K. Kordas¹⁵⁴ G. Koren¹⁵³ A. Korn⁹⁶ I. Korolkov¹⁴ E. V. Korolkova¹⁴¹ N. Korotkova³⁷ O. Kortner¹¹¹
S. Kortner¹¹¹ V. V. Kostyukhin^{141,37} A. Kotsokechagia⁶⁷ A. Kotwal⁵¹ A. Koulouris¹⁰
A. Kourkoumeli-Charalampidi^{73a,73b} C. Kourkoumelis⁹ E. Kourlitis⁶ V. Kouskoura²⁹ R. Kowalewski¹⁶⁷
W. Kozanecki¹⁰² A. S. Kozhin³⁷ V. A. Kramarenko³⁷ G. Kramberger⁹³ D. Krasnopevtsev^{62a} M. W. Krasny¹²⁸
A. Krasznahorkay³⁶ D. Krauss¹¹¹ J. A. Kremer¹⁰¹ J. Kretzschmar⁹² P. Krieger¹⁵⁸ F. Krieter¹¹⁰
A. Krishnan^{63b} M. Krivos¹³⁴ K. Krizka^{18a} K. Kroeninger⁴⁹ H. Kroha¹¹¹ J. Kroll¹³² J. Kroll¹²⁹
K. S. Krowpman¹⁰⁸ U. Kruchonak³⁸ H. Krüger²⁴ N. Krumnack⁸¹ M. C. Kruse⁵¹ J. A. Krzysiak⁸⁶
A. Kubota¹⁵⁷ O. Kuchinskaia³⁷ S. Kuday^{4b} D. Kuechler⁴⁸ J. T. Kuechler⁴⁸ S. Kuehn³⁶ T. Kuhl⁴⁸
V. Kukhtin³⁸ Y. Kulchitsky^{37,k} S. Kuleshov^{138b} Y. P. Kulinich¹⁶⁴ M. Kuna⁶⁰ A. Kupco¹³² T. Kupfer⁴⁹
O. Kuprash⁵⁴ H. Kurashige⁸⁴ L. L. Kurchaninov^{159a} Y. A. Kurochkin³⁷ A. Kurova³⁷ M. G. Kurth^{15a,15d}
E. S. Kuwertz³⁶ M. Kuze¹⁵⁷ A. K. Kvam¹⁴⁰ J. Kvita¹²³ T. Kwan¹⁰⁵ F. La Ruffa^{43b,43a} C. Lacasta¹⁶⁵
F. Lacava^{75a,75b} D. P. J. Lack¹⁰² H. Lacker¹⁹ D. Lacour¹²⁸ E. Ladygin³⁸ R. Lafaye⁵ B. Laforge¹²⁸
T. Lagouri^{138c} S. Lai⁵⁵ I. K. Lakomic^{85a} J. E. Lambert¹²¹ S. Lammers⁶⁸ W. Lampl⁷ C. Lampoudis¹⁵⁴
E. Lançon²⁹ U. Landgraf⁵⁴ M. P. J. Landon⁹⁴ M. C. Lanfermann⁵⁶ V. S. Lang⁵⁴ J. C. Lange⁵⁵
R. J. Langenberg¹⁰⁴ A. J. Lankford¹⁶² F. Lanni²⁹ K. Lantzsch²⁴ A. Lanza^{73a} A. Lapertosa^{57b,57a}
J. F. Laporte¹³⁶ T. Lari^{71a} F. Lasagni Manghi^{23b} M. Lassnig³⁶ T. S. Lau^{65a} A. Laudrain¹⁰¹ A. Laurier³⁴
M. Lavorgna^{72a,72b} S. D. Lawlor⁹⁵ M. Lazzaroni^{71a,71b} B. Le¹⁰² E. Le Guirriec¹⁰³ A. Lebedev⁸¹ M. LeBlanc⁷
T. LeCompte⁶ F. Ledroit-Guillon⁶⁰ A. C. A. Lee⁹⁶ C. A. Lee²⁹ G. R. Lee¹⁷ L. Lee⁶¹ S. C. Lee¹⁵⁰ S. Lee⁸¹
B. Lefebvre^{159a} H. P. Lefebvre⁹⁵ M. Lefebvre¹⁶⁷ C. Leggett^{18a} K. Lehmann¹⁴⁴ N. Lehmann²⁰
G. Lehmann Miotto³⁶ W. A. Leight⁴⁸ A. Leisos^{154,bb} M. A. L. Leite^{82c} C. E. Leitgeb¹¹⁰ R. Leitner¹³⁴
K. J. C. Leney⁴⁴ T. Lenz²⁴ S. Leone^{74a} C. Leonidopoulos⁵² A. Leopold¹²⁸ C. Leroy¹⁰⁹ R. Les¹⁰⁸
C. G. Lester³² M. Levchenko³⁷ J. Levêque⁵ D. Levin¹⁰⁷ L. J. Levinson¹⁷¹ D. J. Lewis²¹ B. Li^{15b} B. Li¹⁰⁷
C-Q. Li^{62a} F. Li^{62c} H. Li^{62a} H. Li^{62b} J. Li^{62c} K. Li¹⁴⁰ L. Li^{62c} M. Li^{15a,15d} Q. Li^{15a,15d} Q. Y. Li^{62a}
S. Li^{62d,62c} X. Li⁴⁸ Y. Li⁴⁸ Z. Li^{62b} Z. Li¹²⁷ Z. Li¹⁰⁵ Z. Liang^{15a} M. Liberatore⁴⁸ B. Liberti^{76a}
A. Liblong¹⁵⁸ K. Lie^{65c} S. Lim²⁹ C. Y. Lin³² K. Lin¹⁰⁸ R. A. Linck⁶⁸ R. E. Lindley⁷ J. H. Lindon²¹
A. Linss⁴⁸ A. L. Lioni⁵⁶ E. Lipeles¹²⁹ A. Lipniacka¹⁷ T. M. Liss^{164,cc} A. Lister¹⁶⁶ J. D. Little⁸ B. Liu⁸¹
B. X. Liu¹⁴⁴ H. B. Liu²⁹ J. B. Liu^{62a} J. K. K. Liu³⁹ K. Liu^{62d,62c} M. Liu^{62a} M. Y. Liu^{62a} P. Liu^{15a} X. Liu^{62a}
Y. Liu⁴⁸ Y. Liu^{15a,15d} Y. L. Liu¹⁰⁷ Y. W. Liu^{62a} M. Livan^{73a,73b} A. Lleres⁶⁰ J. Llorente Merino¹⁴⁴
S. L. Lloyd⁹⁴ C. Y. Lo^{65b} E. M. Lobodzinska⁴⁸ P. Loch⁷ S. Loffredo^{76a,76b} T. Lohse¹⁹ K. Lohwasser¹⁴¹
M. Lokajicek^{132,a} J. D. Long¹⁶⁴ R. E. Long⁹¹ I. Longarini^{75a,75b} L. Longo³⁶ K. A.Looper¹²⁰ I. Lopez Paz¹⁰²
A. Lopez Solis¹⁴¹ J. Lorenz¹¹⁰ N. Lorenzo Martinez⁵ A. M. Lory¹¹⁰ P. J. Lösel¹¹⁰ A. Lösle⁵⁴ X. Lou^{47a,47b}
X. Lou^{15a,15d} A. Lounis⁶⁷ J. Love⁶ P. A. Love⁹¹ J. J. Lozano Bahilo¹⁶⁵ M. Lu^{62a} Y. J. Lu⁶⁶ H. J. Lubatti¹⁴⁰
C. Luci^{75a,75b} F. L. Lucio Alves^{15c} A. Lucotte⁶⁰ F. Luehring⁶⁸ I. Luise¹²⁸ L. Luminari^{75a} B. Lund-Jensen¹⁴⁶
M. S. Lutz¹⁵³ D. Lynn²⁹ H. Lyons⁹² R. Lysak¹³² E. Lytken⁹⁸ F. Lyu^{15a} V. Lyubushkin³⁸ T. Lyubushkina³⁸
H. Ma²⁹ L. L. Ma^{62b} Y. Ma⁹⁶ D. M. Mac Donell¹⁶⁷ G. Maccarrone⁵³ A. Macchiolo¹¹¹ C. M. Macdonald¹⁴¹
J. C. MacDonald¹⁴¹ J. Machado Miguens¹²⁹ D. Madaffari¹⁶⁵ R. Madar⁴⁰ W. F. Mader⁵⁰
M. Madugoda Ralalage Don¹²² N. Madysa⁵⁰ J. Maeda⁸⁴ T. Maeno²⁹ M. Maerker⁵⁰ V. Magerl⁵⁴ N. Magini⁸¹
J. Magro^{69a,69c,dd} D. J. Mahon⁴¹ C. Maidantchik^{82b} T. Maier¹¹⁰ A. Maio^{131a,131b,131d} K. Maj^{85a} O. Majersky^{28a}
S. Majewski¹²⁴ Y. Makida⁸³ N. Makovec⁶⁷ B. Malaescu¹²⁸ Pa. Malecki⁸⁶ V. P. Maleev³⁷ F. Malek⁶⁰
D. Malito^{43b,43a} U. Mallik⁸⁰ D. Malon⁶ C. Malone³² S. Maltezos¹⁰ S. Malyukov³⁸ J. Mamuzic¹⁶⁵

G. Mancini^{72a,72b} I. Mandić⁹³ L. Manhaes de Andrade Filho^{82a} I. M. Maniatis¹⁵⁴ J. Manjarres Ramos⁵⁰
 K. H. Mankinen⁹⁸ A. Mann¹¹⁰ A. Manousos⁷⁹ B. Mansoulie¹³⁶ I. Manthos¹⁵⁴ S. Manzoni¹¹⁶
 A. Marantis^{154,bb} G. Marceca³⁰ L. Marchese¹²⁷ G. Marchiori¹²⁸ M. Marcisovsky¹³² L. Marcoccia^{76a,76b}
 C. Marcon⁹⁸ M. Marjanovic¹²¹ Z. Marshall^{18a} M. U. F. Martensson¹⁶³ S. Marti-Garcia¹⁶⁵ C. B. Martin¹²⁰
 T. A. Martin¹⁶⁹ V. J. Martin⁵² B. Martin dit Latour¹⁷ L. Martinelli^{77a,77b} M. Martinez^{14,u} P. Martinez Agullo¹⁶⁵
 V. I. Martinez Outschoorn¹⁰⁴ S. Martin-Haugh¹³⁵ V. S. Martoiu^{27b} A. C. Martyniuk⁹⁶ A. Marzin³⁶
 S. R. Maschek¹¹¹ L. Masetti¹⁰¹ T. Mashimo¹⁵⁵ R. Mashinistov³⁷ J. Masik¹⁰² A. L. Maslennikov³⁷
 L. Massa^{23b} P. Massarotti^{72a,72b} P. Mastrandrea^{74a,74b} A. Mastroberardino^{43b,43a} T. Masubuchi¹⁵⁵ D. Matakias²⁹
 A. Matic¹¹⁰ N. Matsuzawa¹⁵⁵ P. Mättig²⁴ J. Maurer^{27b} B. Maček⁹³ D. A. Maximov³⁷ R. Mazini¹⁵⁰
 I. Maznas¹⁵⁴ S. M. Mazza¹³⁷ J. P. Mc Gowan¹⁰⁵ S. P. Mc Kee¹⁰⁷ T. G. McCarthy¹¹¹ W. P. McCormack^{18a}
 E. F. McDonald¹⁰⁶ A. E. McDougall¹¹⁶ J. A. Mcfayden^{18a} G. Mchedlize^{151b} M. A. McKay⁴⁴ K. D. McLean¹⁶⁷
 S. J. McMahan¹³⁵ P. C. McNamara¹⁰⁶ C. J. McNicol¹⁶⁹ R. A. McPherson^{167,o} J. E. Mdhluli^{33e}
 Z. A. Meadows¹⁰⁴ S. Meehan³⁶ T. Megy⁴⁰ S. Mehlhase¹¹⁰ A. Mehta⁹² B. Meirose⁴⁵ D. Melini¹⁵²
 B. R. Mellado Garcia^{33e} J. D. Mellenthin⁵⁵ M. Melo^{28a} F. Meloni⁴⁸ A. Melzer²⁴ E. D. Mendes Gouveia^{131a,131e}
 A. M. Mendes Jacques Da Costa²¹ L. Meng³⁶ X. T. Meng¹⁰⁷ S. Menke¹¹¹ E. Meoni^{43b,43a} S. Mergelmeyer¹⁹
 S. A. M. Merkt¹³⁰ C. Merlassino¹²⁷ P. Mermod^{56,a} L. Merola^{72a,72b} C. Meroni^{71a,71b} G. Merz¹⁰⁷ O. Meshkov³⁷
 J. K. R. Meshreki¹⁴³ J. Metcalfe⁶ A. S. Mete⁶ C. Meyer⁶⁸ J-P. Meyer¹³⁶ M. Michetti¹⁹ R. P. Middleton¹³⁵
 L. Mijović⁵² G. Mikenberg¹⁷¹ M. Mikestikova¹³² M. Mikuž⁹³ H. Mildner¹⁴¹ A. Milic¹⁵⁸ C. D. Milke⁴⁴
 D. W. Miller³⁹ A. Milov¹⁷¹ D. A. Milstead^{47a,47b} R. A. Mina¹⁴⁵ A. A. Minaenko³⁷ I. A. Minashvili^{151b}
 A. I. Mincer¹¹⁸ B. Mindur^{85a} M. Mineev³⁸ Y. Minegishi¹⁵⁵ Y. Mino⁸⁷ L. M. Mir¹⁴ M. Mironova¹²⁷
 K. P. Mistry¹²⁹ T. Mitani¹⁷⁰ J. Mitrevski¹¹⁰ V. A. Mitsou¹⁶⁵ M. Mittal^{62c} O. Miu¹⁵⁸ A. Miucci²⁰
 P. S. Miyagawa⁹⁴ A. Mizukami⁸³ J. U. Mjörnmark⁹⁸ T. Mkrtychyan^{63a} M. Mlynarikova¹³⁴ T. Moa^{47a,47b}
 S. Mobius⁵⁵ K. Mochizuki¹⁰⁹ P. Mogg¹¹⁰ S. Mohapatra⁴¹ R. Moles-Valls²⁴ K. Mönig⁴⁸ E. Monnier¹⁰³
 A. Montalbano¹⁴⁴ J. Montejo Berlingen³⁶ M. Montella⁹⁶ F. Monticelli⁹⁰ N. Morange⁶⁷
 A. L. Moreira De Carvalho^{131a} D. Moreno^{22a} M. Moreno Llacer¹⁶⁵ C. Moreno Martinez¹⁴ P. Morettini^{57b}
 M. Morgenstern¹⁵² S. Morgenstern⁵⁰ D. Mori¹⁴⁴ M. Morii⁶¹ M. Morinaga¹⁷⁰ V. Morisbak¹²⁶
 A. K. Morley³⁶ G. Mornacchi³⁶ A. P. Morris⁹⁶ L. Morvaj¹⁴⁷ P. Moschovakos³⁶ B. Moser¹¹⁶ M. Mosidze^{151b}
 T. Moskalets¹³⁶ J. Moss^{31,ee} E. J. W. Moyse¹⁰⁴ S. Muanza¹⁰³ J. Mueller¹³⁰ R. S. P. Mueller¹¹⁰
 D. Muenstermann⁹¹ G. A. Mullier⁹⁸ D. P. Mungo^{71a,71b} J. L. Munoz Martinez¹⁴ F. J. Munoz Sanchez¹⁰²
 P. Murin^{28b} W. J. Murray^{169,135} A. Murrone^{71a,71b} J. M. Muse¹²¹ M. Muškinja^{18a} C. Mwewa^{33a}
 A. G. Myagkov^{37,k} A. A. Myers¹³⁰ G. Myers⁶⁸ J. Myers¹²⁴ M. Myska¹³³ B. P. Nachman^{18a} O. Nackenhorst⁴⁹
 A. Nag⁵⁰ K. Nagai¹²⁷ K. Nagano⁸³ Y. Nagasaka⁶⁴ J. L. Nagle²⁹ E. Nagy¹⁰³ A. M. Nairz³⁶
 Y. Nakahama¹¹³ K. Nakamura⁸³ T. Nakamura¹⁵⁵ H. Nanjo¹²⁵ F. Napolitano^{63a} R. F. Naranjo Garcia⁴⁸
 R. Narayan⁴⁴ I. Naryshkin³⁷ M. Naseri³⁴ T. Naumann⁴⁸ G. Navarro^{22a} P. Y. Nechaeva³⁷ F. Nechansky⁴⁸
 T. J. Neep²¹ A. Negri^{73a,73b} M. Negrini^{23b} C. Nellist¹¹⁵ C. Nelson¹⁰⁵ M. E. Nelson^{47a,47b} S. Nemecek¹³²
 M. Nessi^{36,ff} M. S. Neubauer¹⁶⁴ F. Neuhaus¹⁰¹ M. Neumann¹⁷³ R. Newhouse¹⁶⁶ P. R. Newman²¹ C. W. Ng¹³⁰
 Y. S. Ng¹⁹ Y. W. Y. Ng¹⁶² B. Ngair^{35e} H. D. N. Nguyen¹⁰³ T. Nguyen Manh¹⁰⁹ E. Nibigira⁴⁰
 R. B. Nickerson¹²⁷ R. Nicolaidou¹³⁶ D. S. Nielsen⁴² J. Nielsen¹³⁷ M. Niemeyer⁵⁵ N. Nikiforou¹¹
 V. Nikolaenko^{37,k} I. Nikolic-Audit¹²⁸ K. Nikolopoulos²¹ P. Nilsson²⁹ H. R. Nindhito⁵⁶ A. Nisati^{75a}
 N. Nishu^{62c} R. Nisius¹¹¹ I. Nitsche⁴⁹ T. Nitta¹⁷⁰ T. Nobe¹⁵⁵ D. L. Noel³² Y. Noguchi⁸⁷ I. Nomidis¹²⁸
 M. A. Nomura²⁹ M. Nordberg³⁶ J. Novak⁹³ T. Novak⁹³ O. Novgorodova⁵⁰ R. Novotny¹³³ L. Nozka¹²³
 K. Ntekas¹⁶² E. Nurse⁹⁶ F. G. Oakham^{34,f} H. Oberlack¹¹¹ J. Ocariz¹²⁸ A. Ochi⁸⁴ I. Ochoa⁴¹
 J. P. Ochoa-Ricoux^{138a} K. O'Connor²⁶ S. Oda⁸⁹ S. Odaka⁸³ S. Oerdek⁵⁵ A. Ogrodnik^{85a} A. Oh¹⁰²
 C. C. Ohm¹⁴⁶ H. Oide¹⁵⁷ M. L. Ojeda¹⁵⁸ Y. Okazaki⁸⁷ M. W. O'Keefe⁹² Y. Okumura¹⁵⁵ A. Olariu^{27b}
 L. F. Oleiro Seabra^{131a} S. A. Olivares Pino^{138a} D. Oliveira Damazio²⁹ J. L. Oliver¹ M. J. R. Olsson¹⁶²
 A. Olszewski⁸⁶ J. Olszowska^{86,a} Ö. O. Öncel²⁴ D. C. O'Neil¹⁴⁴ A. P. O'Neill¹²⁷ A. Onofre^{131a,131e}
 P. U. E. Onyisi¹¹ H. Oppen¹²⁶ R. G. Oreamuno Madriz¹¹⁷ M. J. Oreglia³⁹ G. E. Orellana⁹⁰ D. Orestano^{77a,77b}
 N. Orlando¹⁴ R. S. Orr¹⁵⁸ V. O'Shea⁵⁹ R. Ospanov^{62a} G. Otero y Garzon³⁰ H. Otono⁸⁹ P. S. Ott^{63a}
 G. J. Ottino^{18a} M. Ouchrif^{35d} J. Ouellette²⁹ F. Ould-Saada¹²⁶ A. Ouraou^{136,a} Q. Ouyang^{15a} M. Owen⁵⁹

R. E. Owen¹³⁵ V. E. Ozcan^{12c} N. Ozturk⁸ J. Pacalt¹²³ H. A. Pacey³² A. Pacheco Pages¹⁴ C. Padilla Aranda¹⁴ S. Pagan Griso^{18a} G. Palacino⁶⁸ S. Palazzo⁵² S. Palestini³⁶ M. Palka^{85b} P. Palmi^{85a} C. E. Pandini⁵⁶ J. G. Panduro Vazquez⁹⁵ P. Pani⁴⁸ G. Panizzo^{69a,69c} L. Paolozzi⁵⁶ C. Papadatos¹⁰⁹ K. Papageorgiou^{9,r} S. Parajuli⁴⁴ A. Paramonov⁶ C. Paraskevopoulos¹⁰ D. Paredes Hernandez^{65b} S. R. Paredes Saenz¹²⁷ B. Parida¹⁷¹ T. H. Park¹⁵⁸ A. J. Parker³¹ M. A. Parker³² F. Parodi^{57b,57a} E. W. Parrish¹¹⁷ J. A. Parsons⁴¹ U. Parzefall⁵⁴ L. Pascual Dominguez¹²⁸ V. R. Pascuzzi^{18a} J. M. P. Pasner¹³⁷ F. Pasquali¹¹⁶ E. Pasqualucci^{75a} S. Passaggio^{57b} F. Pastore⁹⁵ P. Pasuwan^{47a,47b} S. Pataria¹⁰¹ J. R. Pater¹⁰² A. Pathak^{172,g} J. Patton⁹² T. Pauly³⁶ J. Pearkes¹⁴⁵ B. Pearson¹¹¹ M. Pedersen¹²⁶ L. Pedraza Diaz¹¹⁵ R. Pedro^{131a} T. Peiffer⁵⁵ S. V. Peleganchuk³⁷ O. Penc¹³² H. Peng^{62a} B. S. Peralva^{82a} M. M. Perego⁶⁷ A. P. Pereira Peixoto^{131a} L. Pereira Sanchez^{47a,47b} D. V. Perepelitsa²⁹ E. Perez Codina^{159a} F. Peri¹⁹ L. Perini^{71a,71b,a} H. Pernegger³⁶ A. Perrevoort¹¹⁶ K. Peters⁴⁸ R. F. Y. Peters¹⁰² B. A. Petersen³⁶ T. C. Petersen⁴² E. Petit¹⁰³ V. Petousis¹³³ A. Petridis¹ C. Petridou¹⁵⁴ F. Petrucci^{77a,77b} M. Pettee¹⁷⁴ N. E. Pettersson¹⁰⁴ K. Petukhova¹³⁴ A. Peyaud¹³⁶ R. Pezoa^{138d} L. Pezzotti^{73a,73b} T. Pham¹⁰⁶ P. W. Phillips¹³⁵ M. W. Phipps¹⁶⁴ G. Piacquadio¹⁴⁷ E. Pianori^{18a} A. Picazio¹⁰⁴ R. H. Pickles¹⁰² R. Piegaia³⁰ D. Pietreanu^{27b} J. E. Pilcher³⁹ A. D. Pilkington¹⁰² M. Pinamonti^{69a,69c} J. L. Pinfold³ C. Pitman Donaldson⁹⁶ M. Pitt¹⁵³ L. Pizzimento^{76a,76b} A. Pizzini¹¹⁶ M.-A. Pleier²⁹ V. Plesanovs⁵⁴ V. Pleskot¹³⁴ E. Plotnikova³⁸ P. Podberczko³⁷ R. Poettgen⁹⁸ R. Poggi⁵⁶ L. Poggioli¹²⁸ I. Pogrebnyak¹⁰⁸ D. Pohl²⁴ I. Pokharel⁵⁵ G. Polesello^{73a} A. Poley^{144,159a} A. Policicchio^{75a,75b} R. Polifka¹³⁴ A. Polini^{23b} C. S. Pollard⁴⁸ V. Polychronakos²⁹ D. Ponomarenko³⁷ L. Pontecorvo³⁶ S. Popa^{27a} G. A. Popeneciu^{27d} L. Portales⁵ D. M. Portillo Quintero⁶⁰ S. Pospisil¹³³ K. Potamianos⁴⁸ I. N. Potrap³⁸ C. J. Potter³² H. Potti¹¹ T. Poulsen⁹⁸ J. Poveda¹⁶⁵ T. D. Powell¹⁴¹ G. Pownall⁴⁸ M. E. Pozo Astigarraga³⁶ A. Prades Ibanez¹⁶⁵ P. Pralavorio¹⁰³ S. Prell⁸¹ D. Price¹⁰² M. Primavera^{70a} M. L. Proffitt¹⁴⁰ N. Proklova³⁷ K. Prokofiev^{65c} S. Protopopescu²⁹ J. Proudfoot⁶ M. Przybycien^{85a} D. Pudzha³⁷ A. Puri¹⁶⁴ P. Puzo⁶⁷ D. Pyatiizbyantseva³⁷ J. Qian¹⁰⁷ Y. Qin¹⁰² A. Quadt⁵⁵ M. Queitsch-Maitland³⁶ M. Racko^{28a} F. Ragusa^{71a,71b} G. Rahal⁹⁹ J. A. Raine⁵⁶ S. Rajagopalan²⁹ A. Ramirez Morales⁹⁴ K. Ran^{15a,15d} D. M. Rauch⁴⁸ F. Rauscher¹¹⁰ S. Rave¹⁰¹ B. Ravina⁵⁹ I. Ravinovich¹⁷¹ J. H. Rawling¹⁰² M. Raymond³⁶ A. L. Read¹²⁶ N. P. Readioff¹⁴¹ M. Reale^{70a,70b} D. M. Rebuffi^{73a,73b} G. Redlinger²⁹ K. Reeves⁴⁵ J. Reichert¹²⁹ D. Reikher¹⁵³ A. Reiss¹⁰¹ A. Rej¹⁴³ C. Rembser³⁶ A. Renardi⁴⁸ M. Renda^{27b} M. B. Rendel¹¹¹ A. G. Rennie⁵⁹ S. Resconi^{71a} E. D. Resseguie^{18a} S. Rettie⁹⁶ B. Reynolds¹²⁰ E. Reynolds²¹ O. L. Rezanova³⁷ P. Reznicek¹³⁴ E. Ricci^{78a,78b} R. Richter¹¹¹ S. Richter⁴⁸ E. Richter-Was^{85b} M. Ridel¹²⁸ P. Rieck¹¹¹ O. Rifki⁴⁸ M. Rijssenbeek¹⁴⁷ A. Rimoldi^{73a,73b} M. Rimoldi⁴⁸ L. Rinaldi^{23b,23a} T. T. Rinn¹⁶⁴ G. Ripellino¹⁴⁶ I. Riu¹⁴ P. Rivadeneira⁴⁸ J. C. Rivera Vergara¹⁶⁷ F. Rizatdinova¹²² E. Rizvi⁹⁴ C. Rizzi³⁶ S. H. Robertson^{105,o} M. Robin⁴⁸ D. Robinson³² C. M. Robles Gajardo^{138d} M. Robles Manzano¹⁰¹ A. Robson⁵⁹ A. Rocchi^{76a,76b} E. Rocco¹⁰¹ C. Roda^{74a,74b} S. Rodriguez Bosca¹⁶⁵ A. M. Rodríguez Vera^{159b} S. Roe³⁶ J. Roggel¹⁷³ O. Røhne¹²⁶ R. Röhrig¹¹¹ R. A. Rojas^{138d} B. Roland⁵⁴ C. P. A. Roland⁶⁸ J. Roloff²⁹ A. Romaniouk³⁷ M. Romano^{23b} N. Rompotis⁹² M. Ronzani¹¹⁸ L. Roos¹²⁸ S. Rosati^{75a} G. Rosin¹⁰⁴ B. J. Rosser¹²⁹ E. Rossi⁴⁸ E. Rossi^{77a,77b} E. Rossi^{72a,72b} L. P. Rossi^{57b} L. Rossini⁴⁸ R. Rosten¹⁴ M. Rotaru^{27b} B. Rottler⁵⁴ D. Rousseau⁶⁷ G. Rovelli^{73a,73b} A. Roy¹¹ D. Roy^{33e} A. Rozanov¹⁰³ Y. Rozen¹⁵² X. Ruan^{33e} T. A. Ruggeri¹ F. Rühr⁵⁴ A. Ruiz-Martinez¹⁶⁵ A. Rummler³⁶ Z. Rurikova⁵⁴ N. A. Rusakovich³⁸ H. L. Russell¹⁰⁵ L. Rustige^{40,49} J. P. Rutherford⁷ E. M. Rüttinger¹⁴¹ M. Rybar¹³⁴ G. Rybkin⁶⁷ E. B. Rye¹²⁶ A. Ryzhov³⁷ J. A. Sabater Iglesias⁴⁸ P. Sabatini⁵⁵ L. Sabetta^{75a,75b} S. Sacerdoti⁶⁷ H. F-W. Sadrozinski¹³⁷ F. Safai Tehrani^{75a} B. Safarzadeh Samani¹⁴⁸ M. Safdari¹⁴⁵ P. Saha¹¹⁷ S. Saha¹⁰⁵ M. Sahinsoy¹¹¹ A. Sahu¹⁷³ M. Saimpert³⁶ M. Saito¹⁵⁵ T. Saito¹⁵⁵ H. Sakamoto¹⁵⁵ D. Salamani⁵⁶ G. Salamanna^{77a,77b} A. Salnikov¹⁴⁵ J. Salt¹⁶⁵ A. Salvador Salas¹⁴ D. Salvatore^{43b,43a} F. Salvatore¹⁴⁸ A. Salvucci^{65a,65b,65c} A. Salzburger³⁶ J. Samarati³⁶ D. Sammel⁵⁴ D. Sampsonidis¹⁵⁴ D. Sampsonidou¹⁵⁴ J. Sánchez¹⁶⁵ A. Sanchez Pineda^{69a,36,69c} H. Sandaker¹²⁶ C. O. Sander⁴⁸ I. G. Sanderswood⁹¹ M. Sandhoff¹⁷³ C. Sandoval^{22b} D. P. C. Sankey¹³⁵ M. Sannino^{57b,57a} Y. Sano¹¹³ A. Sansoni⁵³ C. Santoni⁴⁰ H. Santos^{131a,131b} S. N. Santpur^{18a} A. Santra¹⁶⁵ K. A. Saoucha¹⁴¹ J. G. Saraiva^{131a,131d} J. Sardain¹²⁸ O. Sasaki⁸³ K. Sato¹⁶⁰ F. Sauerburger⁵⁴ E. Sauvan⁵ P. Savard^{158,f} R. Sawada¹⁵⁵ C. Sawyer¹³⁵ L. Sawyer⁹⁷ I. Sayago Galvan¹⁶⁵ C. Sbarra^{23b} A. Sbrizzi^{69a,69c} T. Scanlon⁹⁶ J. Schaarschmidt¹⁴⁰ P. Schacht¹¹¹ D. Schaefer³⁹ L. Schaefer¹²⁹ S. Schaepe³⁶ U. Schäfer¹⁰¹ A. C. Schaffer⁶⁷

D. Schaile¹¹⁰ R. D. Schamberger¹⁴⁷ E. Schanet¹¹⁰ C. Scharf¹⁹ N. Scharmberg¹⁰² V. A. Schegelsky³⁷
 D. Scheirich¹³⁴ F. Schenck¹⁹ M. Schernau¹⁶² C. Schiavi^{57b,57a} L. K. Schildgen²⁴ Z. M. Schillaci²⁶
 E. J. Schioppa^{70a,70b} M. Schioppa^{43b,43a} K. E. Schleicher⁵⁴ S. Schlenker³⁶ K. R. Schmidt-Sommerfeld¹¹¹
 K. Schmieden³⁶ C. Schmitt¹⁰¹ S. Schmitt⁴⁸ L. Schoeffel¹³⁶ A. Schoening^{63b} P. G. Scholer⁵⁴ E. Schopf¹²⁷
 M. Schott¹⁰¹ J. F. P. Schouwenberg¹¹⁵ J. Schovancova³⁶ S. Schramm⁵⁶ F. Schroeder¹⁷³ A. Schulte¹⁰¹
 H-C. Schultz-Coulon^{63a} M. Schumacher⁵⁴ B. A. Schumm¹³⁷ Ph. Schune¹³⁶ A. Schwartzman¹⁴⁵
 T. A. Schwarz¹⁰⁷ Ph. Schwemling¹³⁶ R. Schwienhorst¹⁰⁸ A. Sciandra¹³⁷ G. Sciolla²⁶ M. Scornajenghi^{43b,43a}
 F. Scuri^{74a} F. Scutti¹⁰⁶ L. M. Scyboz¹¹¹ C. D. Sebastiani⁹² P. Seema¹⁹ S. C. Seidel¹¹⁴ A. Seiden¹³⁷
 B. D. Seidlitz²⁹ T. Seiss³⁹ C. Seitz⁴⁸ J. M. Seixas^{82b} G. Sekhniaidze^{72a} S. J. Sekula⁴⁴
 N. Semprini-Cesari^{23b,23a} S. Sen⁵¹ C. Serfon²⁹ L. Serin⁶⁷ L. Serkin^{69a,69b} M. Sessa^{62a} H. Severini¹²¹
 S. Sevova¹⁴⁵ F. Sforza^{57b,57a} A. Sfyrila⁵⁶ E. Shabalina⁵⁵ J. D. Shahinian¹³⁷ N. W. Shaikh^{47a,47b}
 D. Shaked Renous¹⁷¹ L. Y. Shan^{15a} M. Shapiro^{18a} A. Sharma¹²⁷ A. S. Sharma¹ P. B. Shatalov³⁷ K. Shaw¹⁴⁸
 S. M. Shaw¹⁰² M. Shehade¹⁷¹ Y. Shen¹²¹ A. D. Sherman²⁵ P. Sherwood⁹⁶ L. Shi⁹⁶ C. O. Shimmin¹⁷⁴
 Y. Shimogama¹⁷⁰ M. Shimojima¹¹² J. D. Shinner⁹⁵ I. P. J. Shipsey¹²⁷ S. Shirabe¹⁵⁷ M. Shiyakova^{38,gg}
 J. Shlomi¹⁷¹ A. Shmeleva³⁷ M. J. Shochet³⁹ J. Shojaii¹⁰⁶ D. R. Shope¹⁴⁶ S. Shrestha¹²⁰ E. M. Shrif^{33e}
 M. J. Shroff¹⁶⁷ E. Shulga¹⁷¹ P. Sicho¹³² A. M. Sickles¹⁶⁴ E. Sideras Haddad^{33e} O. Sidiropoulou³⁶
 A. Sidoti^{23b} F. Siegert⁵⁰ Dj. Sijacki¹⁶ M. Silva Jr.¹⁷² M. V. Silva Oliveira³⁶ S. B. Silverstein^{47a} S. Simion⁶⁷
 R. Simoniello¹⁰¹ C. J. Simpson-allsoy²¹ S. Simsek^{12b} P. Sinervo¹⁵⁸ V. Sinetckii³⁷ S. Singh¹⁴⁴ M. Sioli^{23b,23a}
 I. Siral¹²⁴ S. Yu. Sivoklov^{37,a} J. Sjölin^{47a,47b} A. Skaf⁵⁵ E. Skorda⁹⁸ P. Skubic¹²¹ M. Slawinska⁸⁶
 K. Sliwa¹⁶¹ R. Slovak¹³⁴ V. Smakhtin¹⁷¹ B. H. Smart¹³⁵ J. Smiesko^{28b} N. Smirnov³⁷ S. Yu. Smirnov³⁷
 Y. Smirnov³⁷ L. N. Smirnova^{37,k} O. Smirnova⁹⁸ E. A. Smith³⁹ H. A. Smith¹²⁷ M. Smizanska⁹¹
 K. Smolek¹³³ A. Smykiewicz⁸⁶ A. A. Snesarev³⁷ H. L. Snoek¹¹⁶ I. M. Snyder¹²⁴ S. Snyder²⁹ R. Sobie^{167,o}
 A. Soffer¹⁵³ A. Sogaard⁵² F. Sohns⁵⁵ C. A. Solans Sanchez³⁶ E. Yu. Soldatov³⁷ U. Soldevila¹⁶⁵
 A. A. Solodkov³⁷ A. Soloshenko³⁸ O. V. Solovyanov³⁷ V. Solovyev³⁷ P. Sommer¹⁴¹ H. Son¹⁶¹ A. Sonay¹⁴
 W. Song¹³⁵ W. Y. Song^{159b} A. Sopczak¹³³ A. L. Sopio⁹⁶ F. Sopkova^{28b} S. Sottocornola^{73a,73b}
 R. Soualah^{69a,69c} D. South⁴⁸ S. Spagnolo^{70a,70b} M. Spalla¹¹¹ M. Spangenberg¹⁶⁹ F. Spanò⁹⁵ D. Sperlich⁵⁴
 T. M. Spieker^{63a} G. Spigo³⁶ M. Spina¹⁴⁸ D. P. Spiteri⁵⁹ M. Spousta¹³⁴ A. Stabile^{71a,71b} R. Stamen^{63a}
 M. Stamenkovic¹¹⁶ A. Stampekis²¹ E. Stanecka⁸⁶ B. Stanislaus¹²⁷ M. M. Stanitzki⁴⁸ M. Stankaityte¹²⁷
 B. Stapf¹¹⁶ E. A. Starchenko³⁷ G. H. Stark¹³⁷ J. Stark⁶⁰ P. Staroba¹³² P. Starovoitov^{63a} S. Stärz¹⁰⁵
 R. Staszewski⁸⁶ G. Stavropoulos⁴⁶ M. Stegler⁴⁸ P. Steinberg²⁹ A. L. Steinhebel¹²⁴ B. Stelzer^{144,159a}
 H. J. Stelzer¹³⁰ O. Stelzer-Chilton^{159a} H. Stenzel⁵⁸ T. J. Stevenson¹⁴⁸ G. A. Stewart³⁶ M. C. Stockton³⁶
 G. Stoicea^{27b} M. Stolarski^{131a} S. Stonjek¹¹¹ A. Straessner⁵⁰ J. Strandberg¹⁴⁶ S. Strandberg^{47a,47b}
 M. Strauss¹²¹ T. Strebler¹⁰³ P. Strizenec^{28b} R. Ströhmer¹⁶⁸ D. M. Strom¹²⁴ R. Stroynowski⁴⁴ A. Strubig⁵²
 S. A. Stucci²⁹ B. Stugu¹⁷ J. Stupak¹²¹ N. A. Styles⁴⁸ D. Su¹⁴⁵ W. Su^{62c,140} X. Su^{62a} V. V. Sulin³⁷
 M. J. Sullivan⁹² D. M. S. Sultan⁵⁶ S. Sultansoy^{4c} T. Sumida⁸⁷ S. Sun¹⁰⁷ X. Sun¹⁰² C. J. E. Suster¹⁴⁹
 M. R. Sutton¹⁴⁸ S. Suzuki⁸³ M. Svatos¹³² M. Swiatlowski^{159a} S. P. Swift² T. Swirski¹⁶⁸ A. Sydorenko¹⁰¹
 I. Sykora^{28a} M. Sykora¹³⁴ T. Sykora¹³⁴ D. Ta¹⁰¹ K. Tackmann^{48,hh} J. Taenzer¹⁵³ A. Taffard¹⁶²
 R. Tafirout^{159a} E. Tagiev³⁷ R. Takashima⁸⁸ K. Takeda⁸⁴ T. Takeshita¹⁴² E. P. Takeva⁵² Y. Takubo⁸³
 M. Talby¹⁰³ A. A. Talyshv³⁷ K. C. Tam^{65b} N. M. Tamir¹⁵³ J. Tanaka¹⁵⁵ R. Tanaka⁶⁷ S. Tapia Araya¹⁶⁴
 S. Tapprogge¹⁰¹ A. Tarek Abouelfadl Mohamed¹⁰⁸ S. Tarem¹⁵² K. Tariq^{62b} G. Tarna^{27b,ii} G. F. Tartarelli^{71a}
 P. Tas¹³⁴ M. Tasevsky¹³² E. Tassi^{43b,43a} A. Tavares Delgado^{131a} Y. Tayalati^{35e} A. J. Taylor⁵² G. N. Taylor¹⁰⁶
 W. Taylor^{159b} H. Teagle⁹² A. S. Tee⁹¹ R. Teixeira De Lima¹⁴⁵ P. Teixeira-Dias⁹⁵ H. Ten Kate³⁶ J. J. Teoh¹¹⁶
 K. Terashi¹⁵⁵ J. Terron¹⁰⁰ S. Terzo¹⁴ M. Testa⁵³ R. J. Teuscher^{158,o} S. J. Thais¹⁷⁴ N. Themistokleous⁵²
 T. Thevenaux-Pelzer⁴⁸ F. Thiele⁴² D. W. Thomas⁹⁵ J. O. Thomas⁴⁴ J. P. Thomas²¹ E. A. Thompson⁴⁸
 P. D. Thompson²¹ E. Thomson¹²⁹ E. J. Thorpe⁹⁴ R. E. Ticse Torres⁵⁵ V. Tikhomirov^{37,k} Yu. A. Tikhonov³⁷
 S. Timoshenko³⁷ P. Tipton¹⁷⁴ S. Tisserant¹⁰³ K. Todome^{23b,23a} S. Todorova-Nova¹³⁴ S. Todt⁵⁰ J. Tojo⁸⁹
 S. Tokár^{28a} K. Tokushuku⁸³ E. Tolley¹²⁰ R. Tombs³² K. G. Tomiwa^{33e} M. Tomoto^{83,113} L. Tompkins^{145,jj}
 P. Tornambe¹⁰⁴ E. Torrence¹²⁴ H. Torres⁵⁰ E. Torró Pastor¹⁶⁵ C. Tosciri¹²⁷ J. Toth^{103,kk} D. R. Tovey¹⁴¹
 A. Traet¹⁷ C. J. Treado¹¹⁸ T. Trefzger¹⁶⁸ F. Tresoldi¹⁴⁸ A. Tricoli²⁹ I. M. Trigger^{159a} S. Trincaz-Duvoid¹²⁸

D. A. Trischuk¹⁶⁶ B. Trocmé⁶⁰ A. Trofymov⁶⁷ C. Troncon^{71a} F. Trovato¹⁴⁸ L. Truong^{33c} M. Trzebinski⁸⁶
A. Trzupek⁸⁶ F. Tsai⁴⁸ J. C.-L. Tseng¹²⁷ P. V. Tsiareshka^{37,k} A. Tsirigotis^{154,bb} V. Tsiskaridze¹⁴⁷
E. G. Tskhadadze^{151a} M. Tsopoulou¹⁵⁴ I. I. Tsukerman³⁷ V. Tsulaia^{18a} S. Tsuno⁸³ D. Tsybychev¹⁴⁷ Y. Tu^{65b}
A. Tudorache^{27b} V. Tudorache^{27b} T. T. Tulbure^{27a} A. N. Tuna⁶¹ S. Turchikhin³⁸ D. Turgeman¹⁷¹
I. Turk Cakir^{4b,II} R. J. Turner²¹ R. Turra^{71a} P. M. Tuts⁴¹ S. Tzamarias¹⁵⁴ E. Tzovara¹⁰¹ K. Uchida¹⁵⁵
F. Ukegawa¹⁶⁰ G. Unal³⁶ M. Unal¹¹ A. Undrus²⁹ G. Unel¹⁶² F. C. Ungaro¹⁰⁶ Y. Unno⁸³ K. Uno¹⁵⁵
J. Urban^{28b} P. Urquijo¹⁰⁶ G. Usai⁸ Z. Uysal^{12d} V. Vacek¹³³ B. Vachon¹⁰⁵ K. O. H. Vadla¹²⁶ T. Vafeiadis³⁶
A. Vaidya⁹⁶ C. Valderanis¹¹⁰ E. Valdes Santurio^{47a,47b} M. Valente⁵⁶ S. Valentinetti^{23b,23a} A. Valero¹⁶⁵
L. Valéry⁴⁸ R. A. Vallance²¹ A. Vallier³⁶ J. A. Valls Ferrer¹⁶⁵ T. R. Van Daalen¹⁴ P. Van Gemmeren⁶
S. Van Stroud⁹⁶ I. Van Vulpen¹¹⁶ M. Vanadia^{76a,76b} W. Vandelli³⁶ M. Vandembroucke¹³⁶ E. R. Vandewall¹²²
A. Vaniachine³⁷ D. Vannicola^{75a,75b} R. Vari^{75a} E. W. Varnes⁷ C. Varni^{57b,57a} T. Varol¹⁵⁰ D. Varouchas⁶⁷
K. E. Varvell¹⁴⁹ M. E. Vasile^{27b} G. A. Vasquez¹⁶⁷ F. Vazeille⁴⁰ D. Vazquez Furelos¹⁴ T. Vazquez Schroeder³⁶
J. Veatch⁵⁵ V. Vecchio¹⁰² M. J. Veen¹¹⁶ L. M. Veloce¹⁵⁸ F. Veloso^{131a,131c} S. Veneziano^{75a} A. Ventura^{70a,70b}
A. Verbytskyi¹¹¹ V. Vercesi^{73a} M. Verducci^{74a,74b} C. M. Vergel Infante⁸¹ C. Vergis²⁴ W. Verkerke¹¹⁶
A. T. Vermeulen¹¹⁶ J. C. Vermeulen¹¹⁶ C. Vernieri¹⁴⁵ P. J. Verschuuren⁹⁵ M. C. Vetterli^{144,f} N. Viaux Maira^{138d}
T. Vickey¹⁴¹ O. E. Vickey Boeriu¹⁴¹ G. H. A. Viehhauser¹²⁷ L. Vigani^{63b} M. Villa^{23b,23a} M. Villaplana Perez³
E. M. Villhauer⁵² E. Vilucchi⁵³ M. G. Vincter³⁴ G. S. Virdee²¹ A. Vishwakarma⁵² C. Vittori^{23b,23a}
I. Vivarelli¹⁴⁸ M. Vogel¹⁷³ P. Vokac¹³³ S. E. von Buddenbrock^{33e} E. Von Toerne²⁴ V. Vorobel¹³⁴
K. Vorobev³⁷ M. Vos¹⁶⁵ J. H. Vosseveld⁹² M. Vozak¹⁰² N. Vranjes¹⁶ M. Vranjes Milosavljevic¹⁶ V. Vrba^{133,a}
M. Vreeswijk¹¹⁶ R. Vuillermet³⁶ I. Vukotic³⁹ S. Wada¹⁶⁰ P. Wagner²⁴ W. Wagner¹⁷³ J. Wagner-Kuhr¹¹⁰
S. Wahdan¹⁷³ H. Wahlberg⁹⁰ R. Wakasa¹⁶⁰ V. M. Walbrecht¹¹¹ J. Walder¹³⁵ R. Walker¹¹⁰ S. D. Walker⁹⁵
W. Walkowiak¹⁴³ V. Wallangen^{47a,47b} A. M. Wang⁶¹ A. Z. Wang¹⁷² C. Wang^{62a} C. Wang^{62c} F. Wang¹⁷²
H. Wang^{18a} H. Wang³ J. Wang^{65a} P. Wang⁴⁴ Q. Wang¹²¹ R.-J. Wang¹⁰¹ R. Wang^{62a} R. Wang⁶
S. M. Wang¹⁵⁰ W. T. Wang^{62a} W. X. Wang^{62a} Y. Wang^{62a} Z. Wang¹⁰⁷ A. Warburton¹⁰⁵ C. P. Ward³²
R. J. Ward²¹ N. Warrack⁵⁹ A. T. Watson²¹ M. F. Watson²¹ G. Watts¹⁴⁰ B. M. Waugh⁹⁶ A. F. Webb¹¹
C. Weber²⁹ M. S. Weber²⁰ S. A. Weber³⁴ S. M. Weber^{63a} A. R. Weidberg¹²⁷ J. Weingarten⁴⁹ M. Weirich¹⁰¹
C. Weiser⁵⁴ P. S. Wells³⁶ T. Wenaus²⁹ B. Wendland⁴⁹ T. Wengler³⁶ S. Wenig³⁶ N. Wermes²⁴
M. Wessels^{63a} T. D. Weston²⁰ K. Whalen¹²⁴ A. M. Wharton⁹¹ A. S. White¹⁰⁷ A. White⁸ M. J. White¹
D. Whiteson¹⁶² B. W. Whitmore⁹¹ W. Wiedenmann¹⁷² C. Wiel⁵⁰ M. Wielers¹³⁵ N. Wieseotte¹⁰¹
C. Wiglesworth⁴² L. A. M. Wiik-Fuchs⁵⁴ H. G. Wilkens³⁶ L. J. Wilkins⁹⁵ H. H. Williams¹²⁹ S. Williams³²
S. Willocq¹⁰⁴ P. J. Windischhofer¹²⁷ I. Wingerter-Seez⁵ E. Winkels¹⁴⁸ F. Winklmeier¹²⁴ B. T. Winter⁵⁴
M. Wittgen¹⁴⁵ M. Wobisch⁹⁷ A. Wolf¹⁰¹ R. Wölker¹²⁷ J. Wollrath⁵⁴ M. W. Wolter⁸⁶ H. Wolters^{131a,131c}
V. W. S. Wong¹⁶⁶ N. L. Woods¹³⁷ S. D. Worm⁴⁸ B. K. Wosiek⁸⁶ K. W. Woźniak⁸⁶ K. Wraight⁵⁹ S. L. Wu¹⁷²
X. Wu⁵⁶ Y. Wu^{62a} J. Wuerzinger¹²⁷ T. R. Wyatt¹⁰² B. M. Wynne⁵² S. Xella⁴² J. Xiang^{65c} X. Xiao¹⁰⁷
X. Xie^{62a} I. Xiotidis¹⁴⁸ D. Xu^{15a} H. Xu^{62a} H. Xu^{62a} L. Xu²⁹ T. Xu^{62a} W. Xu¹⁰⁷ Z. Xu^{62b} Z. Xu¹⁴⁵
B. Yabsley¹⁴⁹ S. Yacoob^{33a} D. P. Yallup⁹⁶ N. Yamaguchi⁸⁹ Y. Yamaguchi¹⁵⁷ A. Yamamoto⁸³ M. Yamatani¹⁵⁵
T. Yamazaki¹⁵⁵ Y. Yamazaki⁸⁴ J. Yan^{62c} Z. Yan²⁵ H. J. Yang^{62c,62d} H. T. Yang^{18a} S. Yang^{62a} T. Yang^{65c}
X. Yang^{62b,60} Y. Yang¹⁵⁵ Z. Yang^{62a,107} W.-M. Yao^{18a} Y. C. Yap⁴⁸ E. Yatsenko^{62c} H. Ye^{15c} J. Ye⁴⁴
S. Ye²⁹ I. Yeletsikh³⁸ M. R. Yexley⁹¹ E. Yigitbasi²⁵ P. Yin⁴¹ K. Yorita¹⁷⁰ K. Yoshihara⁸¹ C. J. S. Young³⁶
C. Young¹⁴⁵ J. Yu⁸¹ R. Yuan^{62b,mm} X. Yue^{63a} M. Zaazoua^{35e} B. Zabinski⁸⁶ G. Zacharis¹⁰ E. Zaffaroni⁵⁶
T. Zakareishvili^{151b} N. Zakharchuk³⁴ S. Zambito³⁶ D. Zanzi³⁶ S. V. Zeiβner⁴⁹ C. Zeitnitz¹⁷³ G. Zemaityte¹²⁷
J. C. Zeng¹⁶⁴ O. Zenin³⁷ T. Ženiš^{28a} D. Zerwas⁶⁷ M. Zgubič¹²⁷ B. Zhang^{15c} D. F. Zhang^{15b} G. Zhang^{15b}
J. Zhang⁶ K. Zhang^{15a,15d} L. Zhang^{15c} L. Zhang^{62a} M. Zhang¹⁶⁴ R. Zhang¹⁷² S. Zhang¹⁰⁷ X. Zhang^{62c}
X. Zhang^{62b} Y. Zhang^{15a,15d} Z. Zhang^{65a} Z. Zhang⁶⁷ P. Zhao⁵¹ Z. Zhao^{62a} A. Zhemchugov³⁸ Z. Zheng¹⁰⁷
D. Zhong¹⁶⁴ B. Zhou¹⁰⁷ C. Zhou¹⁷² H. Zhou⁷ M. S. Zhou^{15a,15d} M. Zhou¹⁴⁷ N. Zhou^{62c} Y. Zhou⁷
C. G. Zhu^{62b} C. Zhu^{15a,15d} H. L. Zhu^{62a} H. Zhu^{15a} J. Zhu¹⁰⁷ Y. Zhu^{62a} X. Zhuang^{15a} K. Zhukov³⁷
V. Zhulanov³⁷ D. Zieminska⁶⁸ N. I. Zimine³⁸ S. Zimmermann^{54,a} Z. Zinonos¹¹¹ M. Ziolkowski¹⁴³
L. Živković¹⁶ G. Zobernig¹⁷² A. Zoccoli^{23b,23a} K. Zoch⁵⁵ T. G. Zorbas¹⁴¹ R. Zou³⁹ and L. Zwalinski³⁶

(ATLAS Collaboration)

- ¹*Department of Physics, University of Adelaide, Adelaide, Australia*
²*Physics Department, SUNY Albany, Albany, New York, USA*
³*Department of Physics, University of Alberta, Edmonton, Alberta, Canada*
^{4a}*Department of Physics, Ankara University, Ankara, Türkiye*
^{4b}*Istanbul Aydin University, Application and Research Center for Advanced Studies, Istanbul, Türkiye*
^{4c}*Division of Physics, TOBB University of Economics and Technology, Ankara, Türkiye*
⁵*LAPP, Université Savoie Mont Blanc, CNRS/IN2P3, Annecy, France*
⁶*High Energy Physics Division, Argonne National Laboratory, Argonne, Illinois, USA*
⁷*Department of Physics, University of Arizona, Tucson, Arizona, USA*
⁸*Department of Physics, University of Texas at Arlington, Arlington, Texas, USA*
⁹*Physics Department, National and Kapodistrian University of Athens, Athens, Greece*
¹⁰*Physics Department, National Technical University of Athens, Zografou, Greece*
¹¹*Department of Physics, University of Texas at Austin, Austin, Texas, USA*
^{12a}*Bahcesehir University, Faculty of Engineering and Natural Sciences, Istanbul, Türkiye*
^{12b}*Istanbul Bilgi University, Faculty of Engineering and Natural Sciences, Istanbul, Türkiye*
^{12c}*Department of Physics, Bogazici University, Istanbul, Türkiye*
^{12d}*Department of Physics Engineering, Gaziantep University, Gaziantep, Türkiye*
¹³*Institute of Physics, Azerbaijan Academy of Sciences, Baku, Azerbaijan*
¹⁴*Institut de Física d'Altes Energies (IFAE), Barcelona Institute of Science and Technology, Barcelona, Spain*
^{15a}*Institute of High Energy Physics, Chinese Academy of Sciences, Beijing, China*
^{15b}*Physics Department, Tsinghua University, Beijing, China*
^{15c}*Department of Physics, Nanjing University, Nanjing, China*
^{15d}*University of Chinese Academy of Science (UCAS), Beijing, China*
¹⁶*Institute of Physics, University of Belgrade, Belgrade, Serbia*
¹⁷*Department for Physics and Technology, University of Bergen, Bergen, Norway*
^{18a}*Physics Division, Lawrence Berkeley National Laboratory, Berkeley, California, USA*
^{18b}*University of California, Berkeley, California, USA*
¹⁹*Institut für Physik, Humboldt Universität zu Berlin, Berlin, Germany*
²⁰*Albert Einstein Center for Fundamental Physics and Laboratory for High Energy Physics, University of Bern, Bern, Switzerland*
²¹*School of Physics and Astronomy, University of Birmingham, Birmingham, United Kingdom*
^{22a}*Facultad de Ciencias y Centro de Investigaciones, Universidad Antonio Nariño, Bogotá, Colombia*
^{22b}*Departamento de Física, Universidad Nacional de Colombia, Bogotá, Colombia*
^{23a}*Dipartimento di Fisica e Astronomia A. Righi, Università di Bologna, Bologna, Italy*
^{23b}*INFN Sezione di Bologna, Bologna, Italy*
²⁴*Physikalisches Institut, Universität Bonn, Bonn, Germany*
²⁵*Department of Physics, Boston University, Boston, Massachusetts, USA*
²⁶*Department of Physics, Brandeis University, Waltham, Massachusetts, USA*
^{27a}*Transilvania University of Brasov, Brasov, Romania*
^{27b}*Horia Hulubei National Institute of Physics and Nuclear Engineering, Bucharest, Romania*
^{27c}*Department of Physics, Alexandru Ioan Cuza University of Iasi, Iasi, Romania*
^{27d}*National Institute for Research and Development of Isotopic and Molecular Technologies, Physics Department, Cluj-Napoca, Romania*
^{27e}*University Politehnica Bucharest, Bucharest, Romania*
^{27f}*West University in Timisoara, Timisoara, Romania*
^{28a}*Faculty of Mathematics, Physics and Informatics, Comenius University, Bratislava, Slovak Republic*
^{28b}*Department of Subnuclear Physics, Institute of Experimental Physics of the Slovak Academy of Sciences, Kosice, Slovak Republic*
²⁹*Physics Department, Brookhaven National Laboratory, Upton, New York, USA*
³⁰*Universidad de Buenos Aires, Facultad de Ciencias Exactas y Naturales, Departamento de Física, y CONICET, Instituto de Física de Buenos Aires (IFIBA), Buenos Aires, Argentina*
³¹*California State University, Fresno, California, USA*
³²*Cavendish Laboratory, University of Cambridge, Cambridge, United Kingdom*
^{33a}*Department of Physics, University of Cape Town, Cape Town, South Africa*
^{33b}*iThemba Labs, Western Cape, South Africa*

- ^{33c}*Department of Mechanical Engineering Science, University of Johannesburg, Johannesburg, South Africa*
- ^{33d}*University of South Africa, Department of Physics, Pretoria, South Africa*
- ^{33e}*School of Physics, University of the Witwatersrand, Johannesburg, South Africa*
- ³⁴*Department of Physics, Carleton University, Ottawa, Ontario, Canada*
- ^{35a}*Faculté des Sciences Ain Chock, Réseau Universitaire de Physique des Hautes Energies—Université Hassan II, Casablanca, Morocco*
- ^{35b}*Faculté des Sciences, Université Ibn-Tofail, Kénitra, Morocco*
- ^{35c}*Faculté des Sciences Semlalia, Université Cadi Ayyad, LPHEA-Marrakech, Morocco*
- ^{35d}*LPMR, Faculté des Sciences, Université Mohamed Premier, Oujda, Morocco*
- ^{35e}*Faculté des sciences, Université Mohammed V, Rabat, Morocco*
- ³⁶*CERN, Geneva, Switzerland*
- ³⁷*Affiliated with an institute covered by a cooperation agreement with CERN*
- ³⁸*Affiliated with an international laboratory covered by a cooperation agreement with CERN*
- ³⁹*Enrico Fermi Institute, University of Chicago, Chicago, Illinois, USA*
- ⁴⁰*LPC, Université Clermont Auvergne, CNRS/IN2P3, Clermont-Ferrand, France*
- ⁴¹*Nevis Laboratory, Columbia University, Irvington, New York, USA*
- ⁴²*Niels Bohr Institute, University of Copenhagen, Copenhagen, Denmark*
- ^{43a}*Dipartimento di Fisica, Università della Calabria, Rende, Italy*
- ^{43b}*INFN Gruppo Collegato di Cosenza, Laboratori Nazionali di Frascati, Italy*
- ⁴⁴*Physics Department, Southern Methodist University, Dallas, Texas, USA*
- ⁴⁵*Physics Department, University of Texas at Dallas, Richardson, Texas, USA*
- ⁴⁶*National Centre for Scientific Research “Demokritos,” Agia Paraskevi, Greece*
- ^{47a}*Department of Physics, Stockholm University, Stockholm, Sweden*
- ^{47b}*Oskar Klein Centre, Stockholm, Sweden*
- ⁴⁸*Deutsches Elektronen-Synchrotron DESY, Hamburg and Zeuthen, Germany*
- ⁴⁹*Fakultät Physik, Technische Universität Dortmund, Dortmund, Germany*
- ⁵⁰*Institut für Kern- und Teilchenphysik, Technische Universität Dresden, Dresden, Germany*
- ⁵¹*Department of Physics, Duke University, Durham, North Carolina, USA*
- ⁵²*SUPA—School of Physics and Astronomy, University of Edinburgh, Edinburgh, United Kingdom*
- ⁵³*INFN e Laboratori Nazionali di Frascati, Frascati, Italy*
- ⁵⁴*Physikalisches Institut, Albert-Ludwigs-Universität Freiburg, Freiburg, Germany*
- ⁵⁵*II. Physikalisches Institut, Georg-August-Universität Göttingen, Göttingen, Germany*
- ⁵⁶*Département de Physique Nucléaire et Corpusculaire, Université de Genève, Genève, Switzerland*
- ^{57a}*Dipartimento di Fisica, Università di Genova, Genova, Italy*
- ^{57b}*INFN Sezione di Genova, Genova, Italy*
- ⁵⁸*II. Physikalisches Institut, Justus-Liebig-Universität Giessen, Giessen, Germany*
- ⁵⁹*SUPA—School of Physics and Astronomy, University of Glasgow, Glasgow, United Kingdom*
- ⁶⁰*LPSC, Université Grenoble Alpes, CNRS/IN2P3, Grenoble INP, Grenoble, France*
- ⁶¹*Laboratory for Particle Physics and Cosmology, Harvard University, Cambridge, Massachusetts, USA*
- ^{62a}*Department of Modern Physics and State Key Laboratory of Particle Detection and Electronics, University of Science and Technology of China, Hefei, China*
- ^{62b}*Institute of Frontier and Interdisciplinary Science and Key Laboratory of Particle Physics and Particle Irradiation (MOE), Shandong University, Qingdao, China*
- ^{62c}*School of Physics and Astronomy, Shanghai Jiao Tong University, Key Laboratory for Particle Astrophysics and Cosmology (MOE), SKLPPC, Shanghai, China*
- ^{62d}*Tsung-Dao Lee Institute, Shanghai, China*
- ^{63a}*Kirchhoff-Institut für Physik, Ruprecht-Karls-Universität Heidelberg, Heidelberg, Germany*
- ^{63b}*Physikalisches Institut, Ruprecht-Karls-Universität Heidelberg, Heidelberg, Germany*
- ⁶⁴*Faculty of Applied Information Science, Hiroshima Institute of Technology, Hiroshima, Japan*
- ^{65a}*Department of Physics, Chinese University of Hong Kong, Shatin, N.T., Hong Kong, China*
- ^{65b}*Department of Physics, University of Hong Kong, Hong Kong, China*
- ^{65c}*Department of Physics and Institute for Advanced Study, Hong Kong University of Science and Technology, Clear Water Bay, Kowloon, Hong Kong, China*
- ⁶⁶*Department of Physics, National Tsing Hua University, Hsinchu, Taiwan*
- ⁶⁷*IJCLab, Université Paris-Saclay, CNRS/IN2P3, 91405, Orsay, France*
- ⁶⁸*Department of Physics, Indiana University, Bloomington, Indiana, USA*
- ^{69a}*INFN Gruppo Collegato di Udine, Sezione di Trieste, Udine, Italy*
- ^{69b}*ICTP, Trieste, Italy*
- ^{69c}*Dipartimento Politecnico di Ingegneria e Architettura, Università di Udine, Udine, Italy*

- ^{70a}INFN Sezione di Lecce, Lecce, Italy
^{70b}Dipartimento di Matematica e Fisica, Università del Salento, Lecce, Italy
^{71a}INFN Sezione di Milano, Milano, Italy
^{71b}Dipartimento di Fisica, Università di Milano, Milano, Italy
^{72a}INFN Sezione di Napoli, Napoli, Italy
^{72b}Dipartimento di Fisica, Università di Napoli, Napoli, Italy
^{73a}INFN Sezione di Pavia, Pavia, Italy
^{73b}Dipartimento di Fisica, Università di Pavia, Pavia, Italy
^{74a}INFN Sezione di Pisa, Pisa, Italy
^{74b}Dipartimento di Fisica E. Fermi, Università di Pisa, Pisa, Italy
^{75a}INFN Sezione di Roma, Roma, Italy
^{75b}Dipartimento di Fisica, Sapienza Università di Roma, Roma, Italy
^{76a}INFN Sezione di Roma Tor Vergata, Roma, Italy
^{76b}Dipartimento di Fisica, Università di Roma Tor Vergata, Roma, Italy
^{77a}INFN Sezione di Roma Tre, Roma, Italy
^{77b}Dipartimento di Matematica e Fisica, Università Roma Tre, Roma, Italy
^{78a}INFN-TIFPA, Trento, Italy
^{78b}Università degli Studi di Trento, Trento, Italy
⁷⁹Universität Innsbruck, Department of Astro and Particle Physics, Innsbruck, Austria
⁸⁰University of Iowa, Iowa City, Iowa, USA
⁸¹Department of Physics and Astronomy, Iowa State University, Ames, Iowa, USA
^{82a}Departamento de Engenharia Elétrica, Universidade Federal de Juiz de Fora (UFJF), Juiz de Fora, Brazil
^{82b}Universidade Federal do Rio De Janeiro COPPE/EE/IF, Rio de Janeiro, Brazil
^{82c}Instituto de Física, Universidade de São Paulo, São Paulo, Brazil
⁸³KEK, High Energy Accelerator Research Organization, Tsukuba, Japan
⁸⁴Graduate School of Science, Kobe University, Kobe, Japan
^{85a}AGH University of Krakow, Faculty of Physics and Applied Computer Science, Krakow, Poland
^{85b}Marian Smoluchowski Institute of Physics, Jagiellonian University, Krakow, Poland
⁸⁶Institute of Nuclear Physics Polish Academy of Sciences, Krakow, Poland
⁸⁷Faculty of Science, Kyoto University, Kyoto, Japan
⁸⁸Kyoto University of Education, Kyoto, Japan
⁸⁹Research Center for Advanced Particle Physics and Department of Physics, Kyushu University, Fukuoka, Japan
⁹⁰Instituto de Física La Plata, Universidad Nacional de La Plata and CONICET, La Plata, Argentina
⁹¹Physics Department, Lancaster University, Lancaster, United Kingdom
⁹²Oliver Lodge Laboratory, University of Liverpool, Liverpool, United Kingdom
⁹³Department of Experimental Particle Physics, Jožef Stefan Institute and Department of Physics, University of Ljubljana, Ljubljana, Slovenia
⁹⁴School of Physics and Astronomy, Queen Mary University of London, London, United Kingdom
⁹⁵Department of Physics, Royal Holloway University of London, Egham, United Kingdom
⁹⁶Department of Physics and Astronomy, University College London, London, United Kingdom
⁹⁷Louisiana Tech University, Ruston, Louisiana, USA
⁹⁸Fysiska institutionen, Lunds universitet, Lund, Sweden
⁹⁹Centre de Calcul de l'Institut National de Physique Nucléaire et de Physique des Particules (IN2P3), Villeurbanne, France
¹⁰⁰Departamento de Física Teórica C-15 and CIAFF, Universidad Autónoma de Madrid, Madrid, Spain
¹⁰¹Institut für Physik, Universität Mainz, Mainz, Germany
¹⁰²School of Physics and Astronomy, University of Manchester, Manchester, United Kingdom
¹⁰³CPPM, Aix-Marseille Université, CNRS/IN2P3, Marseille, France
¹⁰⁴Department of Physics, University of Massachusetts, Amherst, Massachusetts, USA
¹⁰⁵Department of Physics, McGill University, Montreal, Québec, Canada
¹⁰⁶School of Physics, University of Melbourne, Victoria, Australia
¹⁰⁷Department of Physics, University of Michigan, Ann Arbor, Michigan, USA
¹⁰⁸Department of Physics and Astronomy, Michigan State University, East Lansing, Michigan, USA
¹⁰⁹Group of Particle Physics, University of Montreal, Montreal, Québec, Canada
¹¹⁰Fakultät für Physik, Ludwig-Maximilians-Universität München, München, Germany
¹¹¹Max-Planck-Institut für Physik (Werner-Heisenberg-Institut), München, Germany
¹¹²Nagasaki Institute of Applied Science, Nagasaki, Japan
¹¹³Graduate School of Science and Kobayashi-Maskawa Institute, Nagoya University, Nagoya, Japan

- ¹¹⁴*Department of Physics and Astronomy, University of New Mexico, Albuquerque, New Mexico, USA*
¹¹⁵*Institute for Mathematics, Astrophysics and Particle Physics, Radboud University/Nikhef, Nijmegen, Netherlands*
- ¹¹⁶*Nikhef National Institute for Subatomic Physics and University of Amsterdam, Amsterdam, Netherlands*
¹¹⁷*Department of Physics, Northern Illinois University, DeKalb, Illinois, USA*
¹¹⁸*Department of Physics, New York University, New York, New York, USA*
¹¹⁹*Ochanomizu University, Otsuka, Bunkyo-ku, Tokyo, Japan*
¹²⁰*The Ohio State University, Columbus, Ohio, USA*
- ¹²¹*Homer L. Dodge Department of Physics and Astronomy, University of Oklahoma, Norman, Oklahoma, USA*
¹²²*Department of Physics, Oklahoma State University, Stillwater, Oklahoma, USA*
¹²³*Palacký University, Joint Laboratory of Optics, Olomouc, Czech Republic*
- ¹²⁴*Institute for Fundamental Science, University of Oregon, Eugene, Oregon, USA*
¹²⁵*Graduate School of Science, Osaka University, Osaka, Japan*
¹²⁶*Department of Physics, University of Oslo, Oslo, Norway*
¹²⁷*Department of Physics, Oxford University, Oxford, United Kingdom*
- ¹²⁸*LPNHE, Sorbonne Université, Université Paris Cité, CNRS/IN2P3, Paris, France*
¹²⁹*Department of Physics, University of Pennsylvania, Philadelphia, Pennsylvania, USA*
- ¹³⁰*Department of Physics and Astronomy, University of Pittsburgh, Pittsburgh, Pennsylvania, USA*
^{131a}*Laboratório de Instrumentação e Física Experimental de Partículas—LIP, Lisboa, Portugal*
^{131b}*Departamento de Física, Faculdade de Ciências, Universidade de Lisboa, Lisboa, Portugal*
^{131c}*Departamento de Física, Universidade de Coimbra, Coimbra, Portugal*
^{131d}*Centro de Física Nuclear da Universidade de Lisboa, Lisboa, Portugal*
^{131e}*Departamento de Física, Universidade do Minho, Braga, Portugal*
^{131f}*Departamento de Física Teórica y del Cosmos, Universidad de Granada, Granada, Spain*
- ^{131g}*Dep Física and CEFITEC of Faculdade de Ciências e Tecnologia, Universidade Nova de Lisboa, Caparica, Portugal*
^{131h}*Departamento de Física, Instituto Superior Técnico, Universidade de Lisboa, Lisboa, Portugal*
¹³²*Institute of Physics of the Czech Academy of Sciences, Prague, Czech Republic*
¹³³*Czech Technical University in Prague, Prague, Czech Republic*
- ¹³⁴*Charles University, Faculty of Mathematics and Physics, Prague, Czech Republic*
- ¹³⁵*Particle Physics Department, Rutherford Appleton Laboratory, Didcot, United Kingdom*
¹³⁶*IRFU, CEA, Université Paris-Saclay, Gif-sur-Yvette, France*
¹³⁷*Santa Cruz Institute for Particle Physics, University of California Santa Cruz, Santa Cruz, California, USA*
- ^{138a}*Departamento de Física, Pontificia Universidad Católica de Chile, Santiago, Chile*
^{138b}*Universidad Andres Bello, Department of Physics, Santiago, Chile*
^{138c}*Instituto de Alta Investigación, Universidad de Tarapacá, Arica, Chile*
- ^{138d}*Departamento de Física, Universidad Técnica Federico Santa María, Valparaíso, Chile*
¹³⁹*Universidade Federal de São João del Rei (UFSJ), São João del Rei, Brazil*
¹⁴⁰*Department of Physics, University of Washington, Seattle, Washington, USA*
- ¹⁴¹*Department of Physics and Astronomy, University of Sheffield, Sheffield, United Kingdom*
¹⁴²*Department of Physics, Shinshu University, Nagano, Japan*
¹⁴³*Department Physik, Universität Siegen, Siegen, Germany*
- ¹⁴⁴*Department of Physics, Simon Fraser University, Burnaby, British Columbia, Canada*
¹⁴⁵*SLAC National Accelerator Laboratory, Stanford, California, USA*
¹⁴⁶*Department of Physics, Royal Institute of Technology, Stockholm, Sweden*
- ¹⁴⁷*Departments of Physics and Astronomy, Stony Brook University, Stony Brook, New York, USA*
¹⁴⁸*Department of Physics and Astronomy, University of Sussex, Brighton, United Kingdom*
¹⁴⁹*School of Physics, University of Sydney, Sydney, Australia*
¹⁵⁰*Institute of Physics, Academia Sinica, Taipei, Taiwan*
- ^{151a}*E. Andronikashvili Institute of Physics, Iv. Javakhishvili Tbilisi State University, Tbilisi, Georgia*
^{151b}*High Energy Physics Institute, Tbilisi State University, Tbilisi, Georgia*
¹⁵²*Department of Physics, Technion, Israel Institute of Technology, Haifa, Israel*
- ¹⁵³*Raymond and Beverly Sackler School of Physics and Astronomy, Tel Aviv University, Tel Aviv, Israel*
¹⁵⁴*Department of Physics, Aristotle University of Thessaloniki, Thessaloniki, Greece*
¹⁵⁵*International Center for Elementary Particle Physics and Department of Physics, University of Tokyo, Tokyo, Japan*
- ¹⁵⁶*Graduate School of Science and Technology, Tokyo Metropolitan University, Tokyo, Japan*
¹⁵⁷*Department of Physics, Tokyo Institute of Technology, Tokyo, Japan*

- ¹⁵⁸*Department of Physics, University of Toronto, Toronto, Ontario, Canada*
^{159a}*TRIUMF, Vancouver, British Columbia, Canada*
^{159b}*Department of Physics and Astronomy, York University, Toronto, Ontario, Canada*
¹⁶⁰*Division of Physics and Tomonaga Center for the History of the Universe, Faculty of Pure and Applied Sciences, University of Tsukuba, Tsukuba, Japan*
¹⁶¹*Department of Physics and Astronomy, Tufts University, Medford, Massachusetts, USA*
¹⁶²*Department of Physics and Astronomy, University of California Irvine, Irvine, California, USA*
¹⁶³*Department of Physics and Astronomy, University of Uppsala, Uppsala, Sweden*
¹⁶⁴*Department of Physics, University of Illinois, Urbana, Illinois, USA*
¹⁶⁵*Instituto de Física Corpuscular (IFIC), Centro Mixto Universidad de Valencia—CSIC, Valencia, Spain*
¹⁶⁶*Department of Physics, University of British Columbia, Vancouver, British Columbia, Canada*
¹⁶⁷*Department of Physics and Astronomy, University of Victoria, Victoria, British Columbia, Canada*
¹⁶⁸*Fakultät für Physik und Astronomie, Julius-Maximilians-Universität Würzburg, Würzburg, Germany*
¹⁶⁹*Department of Physics, University of Warwick, Coventry, United Kingdom*
¹⁷⁰*Waseda University, Tokyo, Japan*
¹⁷¹*Department of Particle Physics and Astrophysics, Weizmann Institute of Science, Rehovot, Israel*
¹⁷²*Department of Physics, University of Wisconsin, Madison, Wisconsin, USA*
¹⁷³*Fakultät für Mathematik und Naturwissenschaften, Fachgruppe Physik, Bergische Universität Wuppertal, Wuppertal, Germany*
¹⁷⁴*Department of Physics, Yale University, New Haven, Connecticut, USA*

^aDeceased.

^bAlso at Department of Physics, King's College London, London, United Kingdom.

^cAlso at Istanbul University, Department of Physics, Istanbul, Türkiye.

^dAlso at Instituto de Física Teórica, IFT-UAM/CSIC, Madrid, Spain.

^eAlso at Institute of Physics, Azerbaijan Academy of Sciences, Baku, Azerbaijan.

^fAlso at TRIUMF, Vancouver, British Columbia, Canada.

^gAlso at Department of Physics and Astronomy, University of Louisville, Louisville, Kentucky, USA.

^hAlso at Physics Department, An-Najah National University, Nablus, Palestine.

ⁱAlso at Department of Physics, University of Fribourg, Fribourg, Switzerland.

^jAlso at Departament de Física de la Universitat Autònoma de Barcelona, Barcelona, Spain.

^kAlso at Affiliated with an institute covered by a cooperation agreement with CERN.

^lAlso at The Collaborative Innovation Center of Quantum Matter (CICQM), Beijing, China.

^mAlso at Department of Physics, Ben Gurion University of the Negev, Beer Sheva, Israel.

ⁿAlso at Università di Napoli Parthenope, Napoli, Italy.

^oAlso at Institute of Particle Physics (IPP), Victoria, Canada.

^pAlso at Borough of Manhattan Community College, City University of New York, New York, New York, USA.

^qAlso at Department of Physics, California State University, Fresno, California, USA.

^rAlso at Department of Financial and Management Engineering, University of the Aegean, Chios, Greece.

^sAlso at Centro Studi e Ricerche Enrico Fermi, Rome, Italy.

^tAlso at Department of Physics, California State University, East Bay, California, USA.

^uAlso at Institutio Catalana de Recerca i Estudis Avancats, ICREA, Barcelona, Spain.

^vAlso at IJCLab, Université Paris-Saclay, CNRS/IN2P3, 91405, Orsay, France.

^wAlso at Physikalisches Institut, Albert-Ludwigs-Universität Freiburg, Freiburg, Germany.

^xAlso at University of Chinese Academy of Sciences (UCAS), Beijing, China.

^yAlso at Institute for Mathematics, Astrophysics and Particle Physics, Radboud University/Nikhef, Nijmegen, Netherlands.

^zAlso at Institute of Theoretical Physics, Iliia State University, Tbilisi, Georgia.

^{aa}Also at CERN, Geneva, Switzerland.

^{bb}Also at Hellenic Open University, Patras, Greece.

^{cc}Also at The City College of New York, New York, New York, USA.

^{dd}Also at Dipartimento di Matematica, Informatica e Fisica, Università di Udine, Udine, Italy.

^{ee}Also at Department of Physics, California State University, Sacramento, California, USA.

^{ff}Also at Département de Physique Nucléaire et Corpusculaire, Université de Genève, Genève, Switzerland.

^{gg}Also at Institute for Nuclear Research and Nuclear Energy (INRNE) of the Bulgarian Academy of Sciences, Sofia, Bulgaria.

^{hh}Also at Institut für Experimentalphysik, Universität Hamburg, Hamburg, Germany.

ⁱⁱAlso at CPPM, Aix-Marseille Université, CNRS/IN2P3, Marseille, France.

^{jj}Also at Department of Physics, Stanford University, Stanford, California, USA.

^{kk}Also at Institute for Particle and Nuclear Physics, Wigner Research Centre for Physics, Budapest, Hungary.

^{ll}Also at Giresun University, Faculty of Engineering, Giresun, Türkiye.

^{mmm}Also at Department of Physics and Astronomy, Michigan State University, East Lansing, Michigan, USA.